Nuclear Engineering and Design 140 (1993) 159–192
North-Holland

Prediction of coupled heat and mass transfer in the Fast Reactor cover gas: the C-GAS code

Y.L. Sinai [a,*], I.J. Ford [b], J.C. Barrett [b] and C.F. Clement [b]

[a] *Technology Department, Engineering Development Centre, NNC Ltd, Risley, Warrington, Cheshire WA3 6BZ, United Kingdom*
[b] *Theoretical Studies Department (MMTD), AEA Technology, Harwell Laboratory, Oxfordshire OX11 0RA, United Kingdom*

Received 1 February 1992, revised version 20 December 1992

Pool designs of the Fast Reactor possess an inert cover gas above the hot pool's free surface. Sodium which evaporates from the hot pool is capable not only of condensing onto steel surfaces, but also of nucleating and forming small aerosol particles which interact strongly with thermal radiation. This paper describes the UK method for analysing these coupled heat and mass transfer processes in assessments of integrity of the roof structure and any components which traverse the gas blanket.

1. Introduction

The pool design of the Fast Reactor possesses a nominally stagnant argon gas blanket sandwiched between the free surface of the sodium hot pool and the roof structure [1]. A general arrangement of a typical design is shown in fig. 1. The blanket is well agitated by turbulence associated with the temperature difference between the hot pool beneath the gas and the relatively cold roof structure above the gas. The blanket is penetrated by a number of components, usually vertical, cylindrically shaped, and possessing a broad spectrum of sizes. Often, annular gaps exist around parts of these components, and such features are capable of sustaining thermosyphonic flows. The designer of the roof structure needs to know global and local heat and mass transport rates to the roof in order to assess cooling requirements, thermal stresses within the structure, and the possible influence of sodium deposition on the operation and effectiveness of various features and structural mechanisms [2].

The temperature difference between the sodium pool and the gas bulk leads to considerable evaporation from the sodium free surface, and it is known that the sodium vapour has the capacity not only to condense on cold surfaces but also to nucleate and condense onto small aerosol droplets. These droplets play a major role in the transport of heat to the roof and associated structures, since they interact strongly with thermal radiation, and radiative calculations of the cover gas therefore fall within the realm of radiation in participating media, a topic which is more complex than conventional exchange across transparent media. It should be noted that the cover gas aerosol's optical properties are such that its albedo is very high, i.e. it is an efficient scatterer of radiation.

A consistent strategy for calculating coupled heat and mass transfer in a well-mixed model of the Fast Reactor cover gas was first formulated by Davidson [3]. The strategy called for iterative, coupled calculations of sensible and latent heat exchange at surfaces facing the gas, the temperatures of those surfaces for given thermal characteristics of underlying structures, three-dimensional radiative exchange between surfaces and the aerosol as well as between the surfaces themselves (accounting for the

* Present address: AEA Consultancy Services (SRD), AEA Technology, Culham Laboratory, Oxfordshire OX14 3DB, United Kingdom.

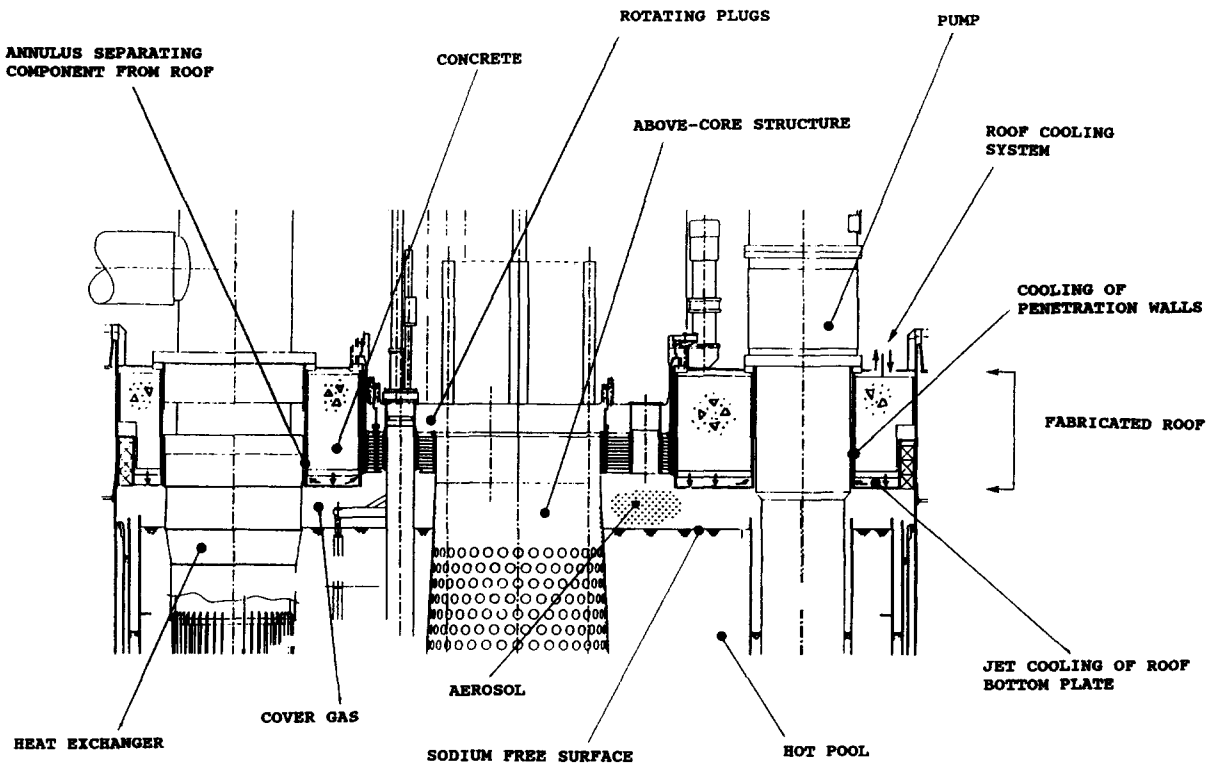

Fig. 1. General arrangement of a typical design in the roof region.

participation of the aerosol), aerosol density and size distribution, aerosol optical properties, and thermosyphonic exchanges with penetrations. The programme leans on the work carried out at the Harwell Laboratories (United Kingdom) by Clement and his colleagues [4–11], particularly in relation to the aerosol behaviour.

The heat and mass transfer processes are coupled because (i) the aerosol mass depends on the evaporation and condensation at bounding surfaces and vice versa (ii) the aerosol particles interact strongly with thermal radiation (iii) sodium deposition influences steel emissivities (iv) vapour transfer and phase change can affect the dynamics of convective motions.

The calculational strategy is encapsulated in the C-GAS code [12], which essentially generalises the Harwell work from a plane-slab model to a three-dimensional analysis of combined convective–radiative heat and mass transfer.

Superficially, this generalisation may sound like an issue of straightforward algebra and computing, but it does, in fact, entail important differences which can fundamentally alter predicted trends and the interpretation of experiments. The significance of this point cannot be over-emphasised and will be illustrated in the discussions below.

Diagrams of the C-GAS strategy and model are presented in figs. 2 and 3. Uniform properties are assumed throughout the cover gas region except for thin boundary layers which are implied at bounding surfaces and, possibly, beneath penetration annuli. Computationally, therefore, C-GAS is a single-node code, but three-dimensional radiation calculations are required.

Thus, after assuming that the cover gas temperature T_g and the aerosol characteristics are uniform in the bulk, the theory needs to address the following:

(i) Sensible and latent convective heat exchange at bounding surfaces.

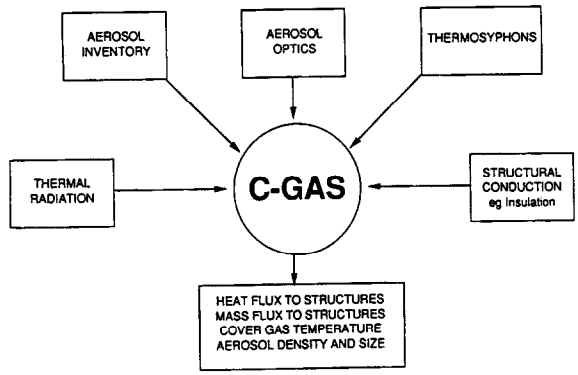

Fig. 2. The C-GAS calculational strategy.

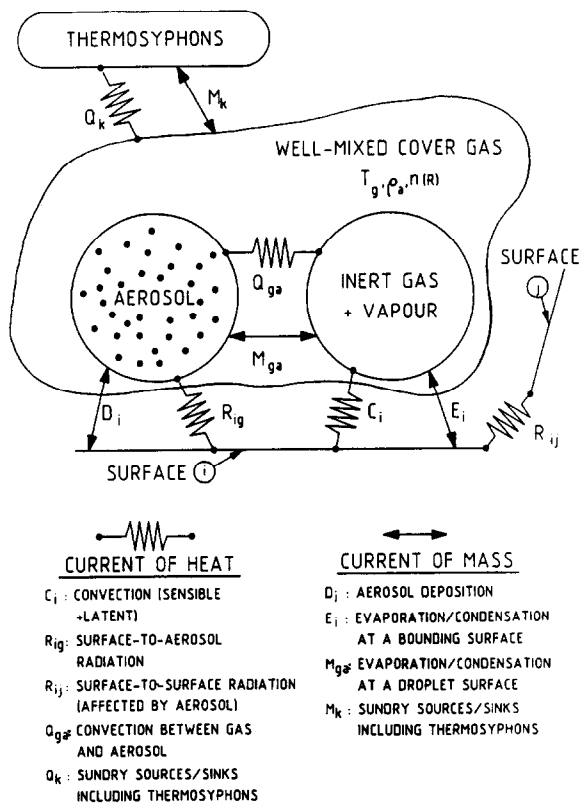

Fig. 3. Sketch of the C-GAS modelling.

(ii) The aerosol inventory, in terms of the size distribution (viz the number of droplets per unit volume as a function of radius).
(iii) The aerosol's optical properties.
(iv) Surface-to-aerosol and surface-to-surface radiative exchange. Note that both aspects are influenced by the aerosol, and that thermodynamic, chemical, and thermal-hydraulic conditions in the cover gas region have a major impact on surface emissivities, as does the make-up of the steel and its history. No attempt shall be made here to review the complex issue of surface emissivities in the presence of sodium vapour and aerosols.
(v) Exchange of heat and mass with narrow regions in which the gas temperature cannot be reasonably characterised by T_g. The most important such locations are the narrow annuli which separate penetrating components from the roof structure, although similar situations may arise beneath the gas blanket too.
(vi) Sometimes, the temperature of a bounding surface is not known a-priori and therefore has to be determined iteratively.

All of the six issues are coupled. Essentially, C-GAS has to perform a global heat balance to determine T_g and surface heat fluxes, coupled to a global mass balance which evaluates the surface mass fluxes as well as the aerosol inventory and optical properties. Some of the six tasks delineated above require a substantial amount of computing (specifically the radiation, the optical properties, and the thermosyphonic losses to roof penetrations). Since C-GAS has to iterate towards the final result (remember that C-GAS is invoked hundreds or thousands of times in a *transient* analysis), it is clear that the most effective approach would utilise separate modules to generate 'look-up tables' for the benefit of C-GAS, which would then synthesize all the tasks with minimal computational effort.

C-GAS-T is a slowly-varying transient version of C-GAS which couples the cover gas to the roof structure (accounting for the thermal inertia of important features) and the natural-convective flows in the roof cooling circuit during postulated passive operation.

A major expedition of the calculations was proposed by [12], where it was argued that the aerosol in a design having an uninsulated roof is likely to be optically thick, and the Optically Thick (OT) radiation model was propounded. In such circumstances the precise value of the optical thickness is unimportant (as long as it is large), and the aerosol's influence on the radiative processes is felt solely through its scattering albedo. This simplifies the radiation calculations dramatically. The isotropically-scaled albedo, which accounts for non-isotropy in the scattering of radiation by sodium particles, was estimated to have a value close to 0.95 on the basis of available information [5].

Superficially, it therefore seems that an aerosol inventory model is superfluous, but several issues militate against this view:

(i) The OT assumption requires corroboration. Support can be found in experimental data, but none of the experiments addressed current design conditions directly. The assumption therefore needs to be backed up by theoretical calculations and experiments
(ii) When the surface emissivity is not small the radiant heat flux is very sensitive to the albedo; the albedo should therefore be calculated
(iii) Design changes can conspire to reduce the aerosol density (e.g. through the use of penetration seals or roof insulation)
(iv) The aerosol mass density has implications for gas cleanup operations and radiological issues
(v) Aerosol deposition can dominate vapour deposition in some circumstances, and can affect surface emissivities.

For these reasons work has continued on the construction of an aerosol model in C-GAS. The physics of aerosols in the cover gas is very complex, particularly in relation to nucleation; heterogeneous mechanisms are believed to be predominantly responsible for the latter, although homogeneous nucleation is not discounted, and this is indeed the least well defined aspect of the theories. The aerosol

modelling which has been adopted for C-GAS is that which has been developed over a period of some years at Harwell, as mentioned above, although for the sake of expedience the preliminary approach outlined here has made a number of simplifying assumptions.

It should be noted that the authors have widened the scope of the strategy to a two-pronged assessment in which the well-mixed concept underlying the C-GAS code is accompanied by a parallel activity which addresses non-uniformities in the cover gas. It is obvious that while vigorous turbulence may be anticipated, the potential for gross circulation and bulk inhomogeneities does exist and may well need to be considered. This activity was named as the 'unmixed model' and a first step along this route has been taken in a one-dimensional analysis of combined transfer in Benard convection [12]; further studies are now under way.

Because of the substantial material involved in the cover gas modelling, this paper is confined to an outline of the theory; a further paper on validation of the code is planned. In a companion paper to the present one [37], numerical examples of computations for a representative geometry are given for illustrative purposes.

2. Some important comments on previous work

As far as previous studies are concerned, the bulk of the published contributions, other than those of the Harwell team, have provided experimental data and some correlations derived therefrom.

A selection of papers published in the open literature may be found in [13–19]. This list reflects the substantial experimental programmes which have been completed in France and Japan. Experimental research, albeit on a smaller scale, has also been conducted, and indeed in some cases is still ongoing, in Britain and Germany. The British cover gas experiments have not been reported in the open literature.

Experimental correlations are useful, provided they are not employed beyond their range of validity. Obviously, a thorough understanding of the basic physical mechanisms involved in sodium–argon heat transfer experiments is required before a satisfactory mathematical model can be formulated. However, the complex behaviour of sodium aerosols and the variability of surface emissivities may, on some occasions, have conspired to obscure the underlying physics. For example [15,16], the radiative flux has often been represented in the following form:

$$q_r = \frac{\sigma\left(T_1^4 - T_2^4\right)}{\dfrac{1}{\epsilon_1} + \dfrac{1}{\epsilon_2} - 1 + \dfrac{3\tau}{4}}. \tag{2.1}$$

Here the subscripts 1 and 2 refer to the hot pool's free surface and roof respectively, and τ is the optical thickness KL where K is the extinction coefficient and L is the vertical separation between the above-mentioned surfaces. The vital point to note is that this formula, based on the diffusion approximation, applies to *pure radiation* [20,21], viz. no other modes of heat transfer exist, the medium's temperature varies across the gap and is part of the solution, and the net fluxes at the boundaries depend on the temperatures of only surfaces 1 and 2. In this formalism, the existence of the aerosol, encapsulated in the last term of the denominator, can only lead to an *attenuation* of radiation in relation to the transparent case. The above papers have attempted to reconcile theory and experiment by considering various combinations of ϵ_1, ϵ_2 and τ in eq. (2.1).

As explained above, however, *multiple* modes of heat transfer are present in the cover gas, and often the bulk of the cover gas is virtually isothermal. Some theories (e.g. [22]), whilst adopting an isothermal profile, have offered sweeping conclusions regarding the significance of the aerosol after ignoring the possible impact of surfaces other than the pool and roof and of penetration thermosyphons, and after

ignoring the major uncertainties in surface emissivities. The significance of all these issues can be easily appreciated [23] by considering a plane-slab geometry with sundry additional transport modes and sources or sinks, such as thermosyphons, capable of changing the bulk temperature. The net radiative flux passing through surface 2 is well approximated by (see section 6 below)

$$q_{2R} = \sigma F_{12}\left(T_1^4 - T_2^4\right) + \sigma F_{2g}\left(T_g^4 - T_2^4\right). \tag{2.2}$$

T_g is the medium's temperature. F_{12} and F_{2g} are view factors which depend, in a complicated fashion, on both surface emissivities and on the medium's optical properties.

The second term, which is missing from (2.1), represents radiation from the aerosol to surface 2: It is capable of overwhelming the first term, and can give rise to an *increase* of heat loading on surface 2 relative to the transparent case. Its omission will lead to incorrect interpretation of experimental observations if an aerosol is present.

It must be reiterated that generally, the medium is in radiative disequilibrium, with the radiative imbalance being exchanged between the aerosol and the carrier gas by conduction (see section 3).

Thus, fundamental differences exist between the above references and the C-GAS modelling. Since C-GAS considers the role of the aerosol in radiative transfer in a general fashion, it is believed to be more versatile and reliable than codes based on restrictive correlations. The predictions of these codes agree with C-GAS in those domains for which the empirical methods are valid. The code which is nearest to C-GAS in its modelling approach is GASMO [24,25]. It utilises the radiation model of Pradel et al. [15], but it does offer an option which is equivalent to the C-GAS optically-thick model, albeit with an overestimated effective gas emissivity of 1.0.

3. The global energy and mass conservations

Due to the assumption used in the well-mixed theory, single 'bulk' values are assigned to the cover gas temperature, the aerosol temperature, and the aerosol properties. Consequently, the macroscopic cover gas energy and (suspended sodium) mass balances are

$$\sum_{i=1}^{m} A_i\left[q_{ic} + \sigma F_{ig}\left(T_i^4 - T_g^4\right)\right] + \sum_{j=1}^{n} Q_j = 0, \tag{3.1}$$

$$\max\left(0, \sum_{i=1}^{m'} A_i E_i\right) - \sum_{j=1}^{n'} M_j = 0. \tag{3.2}$$

Here m is the number of surfaces (each having area A_i) directly facing the cover gas blanket, m' is the number of surfaces at which evaporation is taking place at the rate of E_i kg m^{-2} s^{-1} (condensation corresponds to negative E_i), n is the number of 'extraneous' energy sources such as thermosyphons, and n' is the number of surfaces and phenomena which lead to a removal of sodium at the rate of M_j kg s^{-1}. q_{ic} is the convective heat flux at surface i (see section 3) and F_{ig} is a surface-to-gas configuration factor for the same surface (see section 6). Temperature differences between the aerosol and the gas are assumed to be negligible, but naturally this does not imply that no heat is exchanged between these two media, since the conductance governing the exchange is invariably large.

4. Convective heat transfer at bounding surfaces

The argon–sodium mixture possess a Lewis number which is close to 1; in such circumstances the mass-transfer analogy [26] implies that the total convective (viz. sensible plus latent) heat transfer rate

from surface i to the gas is

$$q_{ic} = h_{ig}(\xi_i - \xi_g), \tag{4.1}$$

where

$$\xi = T + C_e H/C_p. \tag{4.2}$$

Here $C_e(P, T)$ is the sodium vapour's equilibrium mass fraction, $H(T)$ is the sodium latent heat, and C_p is the argon–sodium equilibrium specific heat at constant pressure. h_{ig} is the heat transfer coefficient, which has been assumed to be given by

$$\mathrm{Nu} = \hat{C}\mathrm{Ra}^{\hat{m}}. \tag{4.3}$$

Ra is a Rayleigh number based on $T_i - T_g$, and all physical properties appearing in (4.3) are evaluated at the mean film temperature $(T_i + T_g)/2$, using in-built property tables (see Appendix I).
At present, C-GAS employs

$$\hat{C} = 0.14, \qquad \hat{m} = 1/3. \tag{4.4}$$

These values appertain to turbulent natural-convective flows, of course; there are significant variations in the values reported in the literature, but there is sufficient evidence to support (4.4). It would be a straightforward matter to generalise (4.4), for example to account for differences between vertical and horizontal surfaces or for laminar flows, but these effects are either irrelevant or small in relation to the uncertainties which already exist in the modelling.

It should be noted that while the convective heat flux represented in eq. (4.1) is correct, its breakdown into the sensible and latent components depends on the aerosol characteristics (see section 8).

5. Evaluation of the temperatures of bounding surfaces

5.1. 'Simple' conditions

Preliminary definitions of some terminology would be helpful here. A bounding surface separates the cover gas blanket from the 'world'. The term 'cover gas side' obviously appertains to the domain lying within the cover gas region. The term 'sink side' refers to the complementary region within the 'world'. Note that despite the use of the term 'sink', no direction for the flow of heat across a bounding surface is implied; the sink may be colder or hotter than the surface.

Consider first a straightforward situation where a conductance h_i and sink temperature T_{ic} are specified at surface i, such that the heat flux q_i passing through the surface towards the sink side is $h_i(T_i - T_{ic})$, where T_i is the surface temperature (viz. the temperature at the interface between the structure and the gas). C-GAS iterates for T_i by solving the following equation:

$$q_i - h_i(T_i - T_{ic}) = 0, \tag{5.1.1}$$

where

$$q_i = h_{ig}(\xi_g - \xi_i) + \sigma F_{ig}\left(T_g^4 - T_i^4\right) + \sigma \sum_{j=1}^{m} F_{ji}\left(T_j^4 - T_i^4\right). \tag{5.1.2}$$

The second and third terms in (5.1.2) represent aerosol-to-surface and surface-to-surface radiation respectively (see section 6). It must be emphasised that the view factors are functions of geometry,

surface emissivities, and the aerosol's optical properties. By definition, evaluation of T_i from (5.1.1) thus produces the heat fluxes too.

If the surface temperature is known, h_i should be set to a large number and T_{ic} to the required surface temperature. If the surface flux is to be specified, h_i can be set to (small number) and T_{ic} to the required flux divided by the same small number.

In some circumstances, steel structures emerge from the bounding surface into the cover gas domain. One example concerns the cover gas lying within the ACS (Above-Core Structure) shell, beneath the plug insulation. A large number of vertical shroud tubes traverse the cover gas space and carry heat towards the insulation by conduction and other mechanisms, sometimes independently of conditions in the cover gas space. In order to cope with such circumstances, (5.1.1) and (5.1.2) have been generalised slightly as follows:

$$q_i - h_i(T_i - T_{ic}) - \sigma F_{ic}\left(T_i^4 - \hat{T}_{ic}^4\right) = 0, \tag{5.1.3}$$

$$q_i = (1 - \hat{\alpha}) q_{ig} b + \hat{\alpha} q_{is}, \tag{5.1.4}$$

$$q_{is} = h_{is}(T_{is} - T_i). \tag{5.1.5}$$

In (5.1.4), q_{ig} is the heat flux delivered from the cover-gas to those parts of the surface which face that domain, viz. the expression given by (5.1.2). q_{is} is a heat flux delivered from the same side by the penetrating solid structure. $1 - \hat{\alpha}$ plays the role of a 'porosity' so that $\hat{\alpha}$ is the fraction, in terms of the *total* surface area, which is occupied by the penetrating structure. Naturally, the weighted flux evaluated by (5.1.4) implies that good thermal contact exists between the penetrating structure and the bounding surface. h_{is} and T_{is} are supplied by the user.

For convenience, the last term in (5.1.3) has been incorporated in order to represent radiative exchange between the bounding surface and a sink (on the 'sink' side). Here too, F_{ic} and $\hat{T}_{ic}$ are user-supplied.

Finally, it should be observed that in some circumstances (other than the multiplate/insulation arrangements discussed below) a conductance and sink temperature may be difficult to prescribe because of complex structural geometry and, perhaps, flow conditions on the sink side. A finite-element conduction calculation of the structure may then be necessary.

5.2. Multiplate arrangements

Figure 3 shows a sketch of multiplate arrangements which are often used as insulation. The pack is traversed by a 'bridging' conducting material, for example support studs, or tubes such as those which exist in the ACS region. A 'smeared' one-dimensional model of such arrangements can be calculated by the MPLATE module which is part of the C-GAS code.

Before performing the cover gas calculations, C-GAS computes the performance of the insulation pack (for specified geometry and emissivities) as a function of the temperature of the 'hottest' plate (viz. the plate facing the cover gas), and thereby provides the variation of h_i as a function of T_i; C-GAS subsequently interpolates on these variations, when applying (5.3.1), instead of repeatedly calling MPLATE during the iterations.

Parallel transfer across gas gaps on the one hand, and the bridging material on the other, is represented in a form identical to eq. (5.1.4). Across each gap,

$$q = (1 - \hat{\alpha}) q_g + \hat{\alpha} q_s, \tag{5.2.1}$$

$$q_s = k_s \, \Delta T / X, \tag{5.2.2}$$

$$q_g = q_c + q_R, \tag{5.2.3}$$

Table 1
Natural-convection parameters used in the MPlate module, eq. (4.3)

Orientation	Range of Gr	$\hat{C}$	$\hat{m}$
Horizontal	$Gr < 10^3$	1.0	0
	$10^3 < Gr < 3.2\times10^5$	0.21	1/4
	$3.2\times10^5 < Gr$	0.075	1/3
Vertical	$Gr < 2\times10^3$	1.0	0
	$2\times10^3 < Gr < 2.1\times10^5$	0.20	1/4
	$2.1\times10^5 < Gr$	0.071	1/3

$$q_c = h\ \Delta T, \qquad q_R = \sigma F\left(T_j^4 - T_{j+1}^4\right), \tag{5.2.4}$$

$$F = \left(\epsilon_j^{-1} + \epsilon_{j+1}^{-1} - 1\right)^{-1}. \tag{5.2.5}$$

Here, ΔT is $T_j - T_{j+1}$, where T_j and T_{j+1} represent the smeared temperatures at the two interfaces bounding a gap of depth X. ϵ_j and ϵ_{j+1} are the relevant user-supplied emissivities. k_s is the conductivity of the bridging material, and $\hat{\alpha}$ is the fraction of the total area, normal to the flux lines, which is occupied by that material. h is calculated from a correlation of the form given by (4.3), where Ra is a Rayleigh number based on ΔT and X, and $\hat{C}$ and $\hat{m}$ are supplied in table 1. Physical properties of argon are used, evaluated at the arithmetic mean of T_j and T_{j+1}. Scope exists for adding the effects of sodium to the above modelling.

Refer to fig. 4: The code user specifies the temperatures at the hot end (viz. at interface 1) and the cold end, and the code iterates for the mean heat flux passing through the arrangement. It does this by calculating the $2M - 1$ interface temperatures, where M is the number of plates existing in the Ith pack design (an arbitrary number of pack designs can be represented, and a specific design assigned to each bounding surface). Thus, there are $2M$ unknowns (viz. the interface temperatures and q), and $2M$ algebraic equations set up by applying (5.2.1) in each gap and (5.2.2) in the plates (with X standing for the plate thickness).

MPLATE in fact offers a facility for specifying a 'hot-end temperature' for the radiation term in the first gap which differs from the source utilised for the convection and conduction terms. Also, a value of $\hat{C}$ in (5.2.6) equal to 0.14 can be invoked in the first gap, appropriate to natural-convective exchange with a semi-infinite medium, and in such circumstances the temperature of the first plate (which will possess a small thickness and/or high conductivity) will correspond to the bulk temperature in that medium, and the second plate will represent the 'real' cover plate.

6. Thermal radiation

It is known that for a sufficient temperature difference between the hot pool and the roof structure, sodium vapour condenses to form small sodium droplets. The electromagnetic properties of sodium are such that thermal radiation incident upon the droplets is scattered strongly, and in analysing radiative transfer to the roof features and other structures facing the cover gas it is therefore essential to account for the coupling between the radiation and the aerosol cloud.

This coupling comes under the general heading of 'radiation in participating media'. These processes are governed by the integro-differential radiative transport equation (RTE) (e.g., [20,21]):

$$\frac{1}{K}\boldsymbol{\Omega}\cdot\nabla I_\lambda + I_\lambda = (1-\omega)I_{b\lambda} + \frac{\omega}{4\pi}\int_{4\pi} I_\lambda(\boldsymbol{x}, \boldsymbol{\Omega}')p(\boldsymbol{\Omega}\cdot\boldsymbol{\Omega}')\ \mathrm{d}\Omega'. \tag{6.1}$$

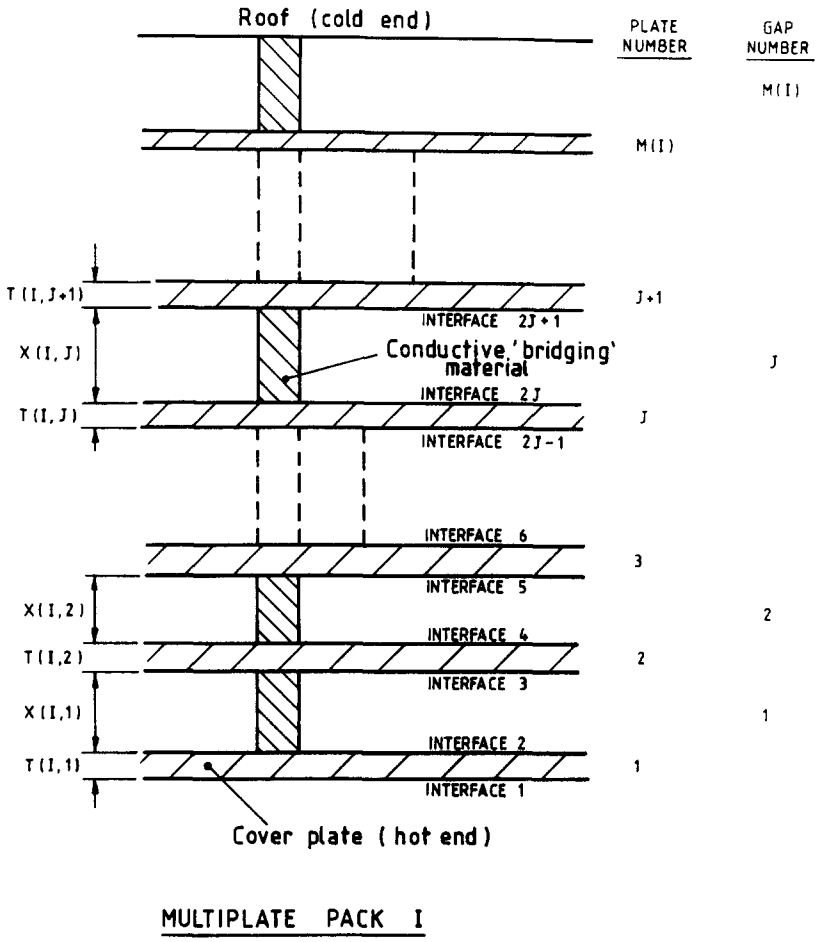

Fig. 4. Conventions used in the MPLATE module.

Here I_λ is the spectral intensity, which is a function of position $\boldsymbol{x}$, direction $\boldsymbol{\Omega}$ and wavelength λ, and $I_{b\lambda}$ is the Planck function. K is the extinction coefficient $K_a + K_s$ (m^{-1}), K_a and K_s are the spectral absorption and scattering coefficients, ω is the scattering albedo K_s/K, and p is the scattering phase function which depends on the angle between the direction $\boldsymbol{\Omega}$ and the dummy direction $\boldsymbol{\Omega}'$ in the scattering integral. The scattering is non-isotropic, but linear scaling can reduce the analysis to an equivalent isotropic calculation (e.g. [5,27]).

The analysis of radiative transfer is simplified very substantially by invoking wavelength-averaged optical properties (see section 9) in a gray-medium approximation. Then eq. (6.1) stands, with $I_{b\lambda}$ and I_λ being replaced by I_b and I (the total intensities). For polydisperse clouds, the absorption and scattering coefficients are found from the size-dependent single-article efficiencies by summing over particle size.

The RTE is known for its complexity, particularly when subjected to combinations of diffuse and specular boundary conditions. The net radiative flux arriving at any of the m surfaces is given by [20]

$$q_{iR} = \sigma F_{ig}\left(T_g^4 - T_i^4\right) + \sigma \sum_{j=1}^{m} F_{ji}\left(T_j^4 - T_i^4\right). \tag{6.2}$$

The view (or configuration) factors F_{ig} and F_{ij} are to be determined from eq. (6.1). Generally, this is a major task, as may be appreciated when it is observed that

$$\left.\begin{matrix} F_{ig} \\ F_{ij} \end{matrix}\right\} = \text{function}\left\{\begin{matrix} \text{geometry, aerosol density,} \\ \text{aerosol size distribution,} \\ \text{surface emissivities.} \end{matrix}\right. \tag{6.3}$$

The reader should note that the F's referred to in this paper are not the common geometric view factors which appear in text book chapters on exchange in transparent cavities. The issue of surface emissivities alone is a difficult topic in its own right, depending as it does on thermal-hydraulics and surface chemistry. As mentioned in the introduction, a dramatic reduction of computing effort has been gained with the OTM (Optically Thick Model); here, $F_{ij} = 0$ and only F_{ig} is significant because the surfaces are not visible to one another. The model was proposed for designs in which the roof is uninsulated, but the validity of the model becomes questionable with the addition of roof insulation and/or penetration seals. The OTM expressions are

$$F_{ig} = \left(\frac{1}{\epsilon_i} + \frac{1}{\epsilon_g} - 1\right)^{-1}, \tag{6.4}$$

$$\epsilon_g = 1 - \left(\frac{2\omega}{\nu^2}\right)\frac{[\nu - \ln(1+\nu)]^2}{\nu - \omega\,\ln(1+\nu)}, \tag{6.5}$$

$$\ln\left(\frac{1+\nu}{1-\nu}\right) - \frac{2\nu}{\omega} = 0. \tag{6.6}$$

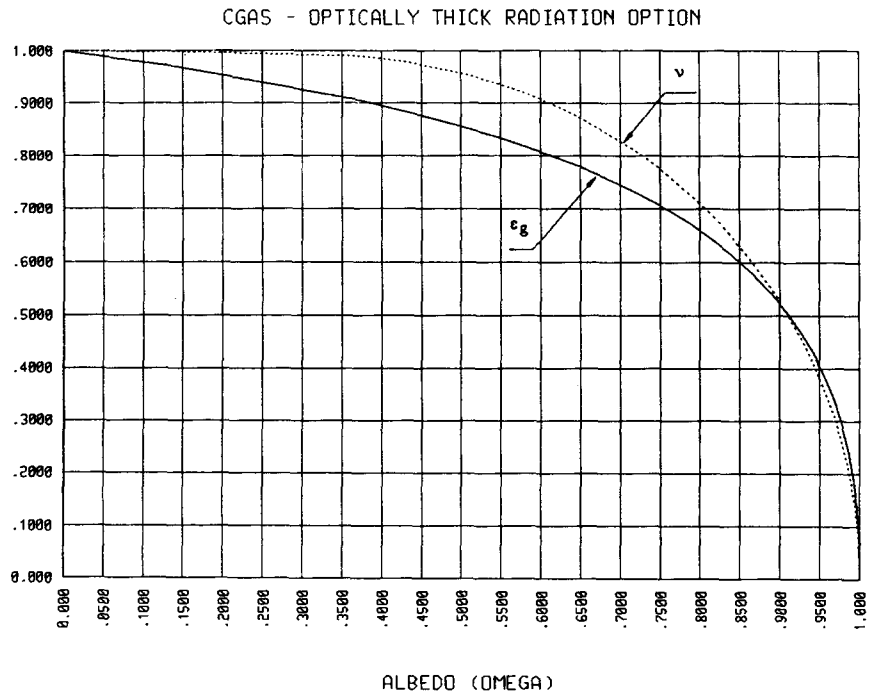

Fig. 5. The optically-thick radiation model. Variations of ϵ_g and ν with ω.

The variation of ϵ_g, an equivalent gas emissivity, as a function of the albedo, is given in Fig. 5. The parameter ν is sometimes named after Chandrasekhar. Thus, if the opacity of the medium is large, its precise value is unimportant, and it is only the albedo which enters the calculations. Note, however that ϵ_g is sensitive to variations in ω when the latter approaches 1.

For plane–slab transfer through a medium having arbitrary optical properties, C-GAS offers the variational formulae of Williams [28]. Expression (6.4) is, in fact, derived therefrom.

Preliminary 3-D calculations have been carried out using the P_1 approximation with radiation slip conditions at boundaries. However, this approximation is known to be inadequate, especially when the medium is not thick, and presently Monte Carlo simulations are being used to evaluate the view factors for a range of opacities, albedos, and emissivities. C-GAS interpolates linearly on the look-up table which is generated by such simulations.

The user is free to interpolate with respect to only the opacity, for a single value of the albedo, or simultaneously with respect to both the opacity and the albedo if the appropriate tables have been provided to the code. For extinction coefficients which are larger than a certain user-supplied value, the OTM is imposed. The number of calculations which are required grows rapidly with the number of surface m, but it will not always be necessary to compute all the view factors. For example, note that

$$A_j F_{ij} = A_i F_{ji}. \tag{6.7}$$

Moreover, if the bounding temperatures are specified, and the heat fluxes are only required at a limited number m'' of the surfaces, then the number of required view factors for each albedo, opacity and emissivity set is reduced to $(m'' + 1)(m - \frac{1}{2}m'')$, and the necessary number of radiation computations is m''.

7. Component penetrations

The components which penetrate the roof structure are separated from the roof by relatively narrow annuli. Generally, the annuli possess adiabatic or warm diabatic inner walls, and relatively cold outer walls. Two extreme flow regimes are possible:

(i) recirculating or 'counter-current' double-glazing flows,

(ii) directed thermosyphonic flows.

Which of these dominates will depend on the geometry and the temperature differences between the inner wall, outer wall, and cover gas, but thermosyphonic flows are more likely in typical annuli. The thermosyphons are influenced by any structural feature which has the potential to alter the wall temperature; the ribs which carry some of the mechanical load and which divide the roof cooling system in the fabricated roof design fall into this category, since they are capable of inducing cold or hot 'patches' on the outer walls. It should be noted that two annuli also exist at the edges of the two rotating plugs. The roof designer also needs to be aware of the inherent instability which drives the thermosyphons, and of the possibility that the flows may fluctuate in a manner which could damage the structure.

Predictions of the annular flows are required for two reasons:

(i) The net heat and mass exchange with the cover gas is required by C-GAS.

(ii) The total and detailed heat loading determines the cooling requirements and thermal stresses in the structure.

With regard to (i), some feel for the magnitude of the penetration losses can be acquired from past C-GAS computations which suggest that while they are fairly sensitive to the roof emissivity (since the latter affects the cover gas and roof cooling temperatures), typical combined losses are about 1/3 of the total heat gained by the roof cooling system.

As far as analysis is concerned, it is of course essential to couple the structural thermal calculations with those of the thermosyphons. It is hoped that eventually, the computer codes which are being used for these two aspects will be fully integrated, but at present, two simpler principal methods are being used. In the first, a structural-thermal analysis is performed with simple boundary conditions at the annulus walls; effectively this provides the conductances h_i and the sink temperatures T_{ic} which are then applied by the fluid flow code. In the second approach, a 'manual' iteration is carried out by alternate computations with the fluid flow and structural codes; the former provides heat fluxes as boundary conditions to the latter, and the latter provides temperatures as boundary conditions to the former.

There is a fairly large number of computer codes which are capable of analysing this situation, varying from simple network models in which the number of lobes has to be specified by the user, to full CFD (Computational Fluid Dynamics) codes capable of solving the full set of fluid dynamics equations (e.g. [29]) with a variety of turbulence models. Due to the fact that a large number of computer runs are required, because of the diversity of penetration types and because C-GAS must be supplied with the *variation* of the net heat loss as a function of cover gas temperature, the decision was made to perform most of the calculations with a general-purpose network code which has been tailored to the Fast Reactor penetration requirements. The code is named PENHEAT. The PENHEAT modelling is based on an integration of the conservation equations across the annulus gap, so that only one cell bridges that gap but arbitrary mesh arrangements are permitted in the azimuthal and vertical directions. Gas-wall exchanges are represented by correlations, and the code adopts the parallel-plate, clear-medium configuration to approximate radiative transfer in the annulus.

As far as C-GAS is concerned, all the above computations are encapsulated in user-supplied routines which specify the variations of the net exchanges between the penetrations and the cover gas (the Q_j's in eq. (3.1)) as functions of T_g. The heat delivered to the outer wall of the annulus differs from the net exchange if the inner wall is not adiabatic.

8. Aerosol inventory

8.1. Background

The aerosol theory [4–11] is intricate, and beside a brief outline of the salient assumptions underlying the model, this section will simply be confined to a summary of the mathematical equations and an explanation of any modifications thereto.

The model addresses a well-stirred cavity in which conditions in the bulk are uniform and gradients of temperature and sodium concentrations appear only at bounding surfaces or at mixing layers. Aerosol formation, growth, or decay are controlled by diffusive currents and will only occur in the vicinity of such currents. Equilibration between a typical droplet and its environment is extremely rapid, and the bulk is at equilibrium unless the vapour and aerosol densities are low; departure from equilibrium is therefore presumed to occur only at boundary and mixing layers.

Several important dimensionless parameters will now be defined.
The supersaturation $\hat{S}$ is given by

$$\hat{S} = P_v/P_{ve}, \tag{8.1.1}$$

where P_v is the local (sodium) vapour pressure and $P_{ve}(T)$ is the equilibrium vapour pressure corresponding to the local value of the mixture temperature T.

The surface condensation number is defined by

$$\mathrm{Cn}(S, T_i, T_g) = \frac{-k\,\nabla T}{\rho H \hat{D}\,\nabla \ln(1-C)} = \frac{q_s}{q_l}. \tag{8.1.2}$$

Here T_i and T_g are the surface (identified by i) and bulk gas temperatures, and the right-hand side of eq. (8.1.2) is evaluated at the surface. q_s and q_l are the sensible and latent heat fluxes respectively. $\hat{D}$ is the binary mass diffusion coefficient, and C is the non-equilibrium vapour mass fraction:

$$C = \rho_v/\rho, \qquad \rho = \rho_v + \rho_g, \tag{8.1.3}$$

where ρ_v and ρ_g are the vapour (sodium) and inert gas (argon) densities respectively. Note that ρ does not include the aerosol density, and that the latter is often much larger than ρ_v. The vapour–argon mixture is assumed to behave as an ideal gas system. Cn is the ratio of sensible heat transport by conduction to latent heat transport by vapour diffusion, and expression (8.1.2) appertains to a mixture in which only one of the species is condensible.

An alternative definition of the supersaturation is

$$S = C/C_e, \tag{8.1.4}$$

where C_e is the equilibrium mass fraction. Differences between $\hat{S}$ and S are small.

Two limits are of interest. At saturation,

$$\hat{\mathrm{Cn}} = \mathrm{Cn}(1, T_i, T_g) = \frac{k(1-C_e)}{\rho H \hat{D} C_e'}, \tag{8.1.5}$$

where prime denotes differentiation with respect to T and all quantities are evaluated at the temperature T_i. The equilibrium limit is approached as the aerosol number density becomes large. The variations of C_e and $\hat{\mathrm{Cn}}$ with temperature and pressure are depicted in fig. 6 (see eq. (8.1.10) below).

In the obverse limit of total decoupling of heat and mass transfer through a boundary layer without any aerosol, the maximum supersaturation is

$$S_m = \frac{1}{C_e(T_m)}\left\{C_e(T_g) + \left[C_e(T_g) - C_e(T_i)\right]\left(\frac{T_m - T_g}{T_g - T_i}\right)\right\}, \tag{8.1.6}$$

where

$$T_m = \frac{B}{2}\left\{1 - \left(1 - \frac{4}{B}\left[\frac{T_i C_e(T_g) - T_g C_e(T_i)}{C_e(T_g) - C_e(T_i)}\right]\right)^{1/2}\right\}. \tag{8.1.7}$$

The parameter B will be explained below. The corresponding condensation number is

$$\mathrm{Cn}_m = \hat{\mathrm{Cn}}(T_i) C_e'(T_i)\left[\frac{T_g - T_i}{C_e(T_g) - C_e(T_i)}\right]. \tag{7.1.8}$$

S_m is plotted in fig. 7, where it is seen that it can vary over many orders of magnitude. The vapour equilibrium density and mass fraction can be evaluated by C-GAS as described in Appendix I, but it is

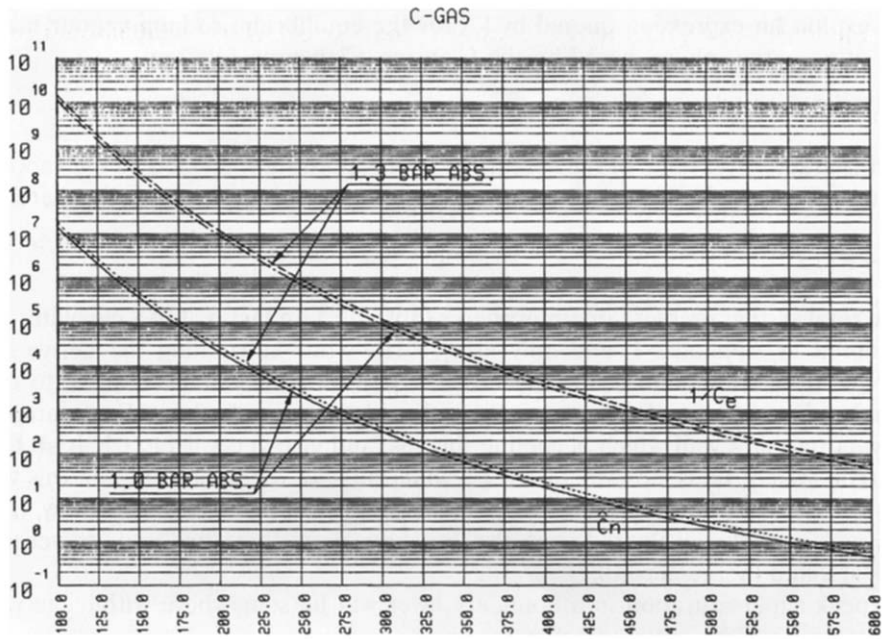

Fig. 6. Variations of the equilibrium surface condensation number $\hat{C}n$ and vapour mass fraction C_e with temperature and pressure.

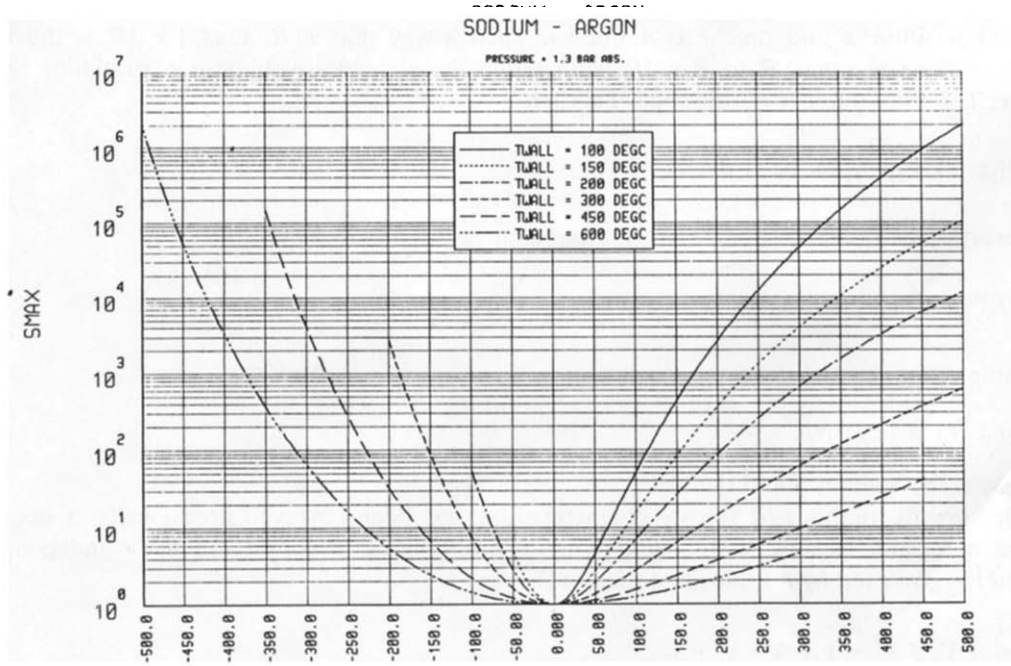

Fig. 7. S_m as a function of $T_g - T_w$, for a range of values of T_w.

convenient to exploit an expression quoted by [7] for the equilibrium sodium vapour mass fraction at a total pressure of one atmosphere, based on the Clausius–Clapeyron relation:

$$\hat{C}_e = A\ e^{-B/T}, \qquad A = 3.5775 \times 10^4,\ B = 1.2565 \times 10^4\ \text{K}. \tag{8.1.9}$$

B represents a characteristic value of the sodium heat of vaporisation divided by the vapour gas constant. Since the mixture is ideal, this can be generalised to pressures other than 1 atmosphere as follows:

$$C_e = \left[1 + P\left(1/\hat{C}_e - 1\right)\right]^{-1}, \tag{8.1.10}$$

where P is the total system pressure in atmospheres (absolute). In fact, C-GAS evaluates C_e with the full expressions quoted in Appendix I, and only uses (8.1.9) when calculating the derivatives of C_e with respect to temperature. It should be mentioned that aerosol behaviour is sensitive to the value of the Lewis number Le, equal to $k/\rho\hat{D}C_p$, where C_p is the mixture specific heat. For example, if Le < 1 an aerosol will evaporate at a wall which is cooling the gas, and vice versa if Le > 1. It so happens that for the sodium–argon system Le is close to 1.0 over a wide range of temperatures, and this value is adopted for present purposes, with the well known implications for the mass transfer analogy. This enables the total convective flux to be evaluated, but the breakdown of that flux into its sensible and latent components is affected by the aerosol.

The actual peak supersaturation in a boundary layer will lie somewhere within the range 1.0 to S_m, and its determination will be outlined below.

8.2. The size distribution and its moments

The droplets are assumed to be spherical, and if R denotes the radius of a droplet, then the number density at position $\boldsymbol{x}$ and time t is defined in such a way that $n(R, \boldsymbol{x}, t)\ \mathrm{d}^3\boldsymbol{x}\ \mathrm{d}R$ is the number of droplets in the size range R to $R + \mathrm{d}R$ lying within the elemental volume $\mathrm{d}^3\boldsymbol{x}$ straddling the position vector $\boldsymbol{x}$. The total number density (m^{-3}) is then

$$N(\boldsymbol{x}, t) = \int_0^\infty n(R, \boldsymbol{x}, t)\ \mathrm{d}R \tag{8.2.1}$$

and the mth mean is defined in terms of a moment of the distribution:

$$N\overline{R^m} = \int_0^\infty n(R, \boldsymbol{x}, t) R^m\ \mathrm{d}R. \tag{8.2.2}$$

For example, the aerosol density ρ_a is given by:

$$\rho_a(\boldsymbol{x}, t) = \tfrac{4}{3}\pi\rho_L N\overline{R^3}, \tag{8.2.3}$$

where ρ_L is the sodium liquid density.

While slow fluctuations of aerosol characteristics have been observed occasionally, a steady state is assumed here, and because of the underlying assumptions, n is considered to be independent of $\boldsymbol{x}$. $n(\boldsymbol{x}, R, t)$ is governed by a Liouville equation [7]:

$$\frac{\partial n}{\partial t} + \nabla\cdot\boldsymbol{J} + \frac{\partial}{\partial R}(\dot{R}n) = \tilde{S}_1 + \tilde{S}_2. \tag{8.2.4}$$

Here $\boldsymbol{J}$ is the spatial aerosol current ($\mathrm{m}^{-3}\ \mathrm{s}^{-1}$), the last term on the left-hand side represents aerosol growth, and $\tilde{S}_1$ and $\tilde{S}_2$ quantify the roles of nucleation and coagulation. Numerical solutions of (8.2.4)

can be found, but C-GAS exploits a closed-form solution which applies when, as is currently assumed, gravitational settling is the dominant aerosol removal mechanism [7]:

$$n = n_0 R \exp(-\alpha R^4). \tag{8.2.5}$$

Here, n_0 and α are constants (to be determined) in a given set of conditions. For this distribution

$$\overline{R^m} = \left(\frac{n_0}{4N}\right)\alpha^{-\tilde{m}}\Gamma(\tilde{m}), \qquad \tilde{m} = \tfrac{1}{4}(m+2), \tag{8.2.6}$$

where Γ is the Gamma function [30]. Write

$$\gamma = N\overline{R}, \tag{8.2.7}$$

then

$$\Gamma(\tfrac{3}{4})n_0 - 4\gamma\alpha^{3/4} = 0. \tag{8.2.8}$$

Note that the latent flux, as a fraction of the total convective flux, is

$$\frac{q_{il}}{q_{ic}} = \frac{1}{1+\mathrm{Cn}_i}. \tag{8.2.9}$$

Remembering that only gravitational settling is considered as an aerosol sink, eq. (3.2) is written as

$$\max\left(0, \sum_{i=1}^{m} \frac{A_i q_{ic}}{H(T_i)(1+\mathrm{Cn}_i)}\right) - M_1 = 0, \tag{8.2.10}$$

where

$$2\pi\rho_L^2 A_s g\gamma - 9\alpha\mu M_1 = 0. \tag{8.2.11}$$

In (8.2.11), A_s is the user-supplied horizontal (or horizontal projection) area over which settling can occur, and μ is the dynamic viscosity of the gaseous phase. The latter is evaluated at the hot pool temperature.

Thus, before the aerosol inventory can be determined, it is necessary to evaluate (as the iterations proceed) all the condensation numbers and γ (the first moment of the distribution). The following sections describe how this is done.

8.3. Near-equilibrium theory

The earlier Harwell theories were based on the assumption of $S-1$ being small at each surface. This condition is true when the aerosol is thick, and this was the first Harwell theory to be implemented in C-GAS.

The equations are

$$S_i - 1 - \left[\frac{q_{ic}\mathrm{Cn}_i}{k(1+\mathrm{Cn}_i)}\right]^2 \frac{C_e''}{4\pi\gamma C_e} = 0, \tag{8.3.1}$$

$$\mathrm{Cn}_i\left[1 + \mathrm{sgn}(T_g - T_i)(S_i-1)^{1/2}(C_e C_e'')^{1/2}/C_e'\right] - \hat{\mathrm{Cn}}_i = 0. \tag{8.3.2}$$

In the above, C_e and its derivatives are evaluated at the appropriate wall temperature. In mathematical terms, eqs. (8.2.7, 9, 10) and (8.3.1, 2) are only $2m+3$ equations for $2m+4$ unknowns (namely S_i, Cn_i,

M_1, $N\bar{R}$, α and n_0), and the present state of knowledge in this field cannot provide a rigorous closure to this system. One variable therefore needs to be assumed, preferably on the basis of experimental observations, and a specification of the supersaturation at the roof is the approach recommended by [7–11]. Once the system of equations is solved, the total number density N and the aerosol mass density ρ_a are found from moments of the distribution (8.2.4):

$$N = \tfrac{1}{4}\Gamma(\tfrac{1}{2})\alpha^{-1/2}n_0, \tag{8.3.3}$$

$$\rho_a = \pi\alpha^{-5/4}\Gamma(5/4)\rho_L n_0/3. \tag{8.3.4}$$

It can be shown from this set of equations that for a system possessing a roof at the relatively low temperature typical of an uninsulated design, the following trends may be obtained:

$$\begin{aligned} &\alpha \propto (S_2 - 1)^{-1}, \\ &n_0 \propto (S_2 - 1)^{-7/4}, \\ &N \propto (S_2 - 1)^{-5/4}, \\ &\rho_a \propto (S_2 - 1)^{-1/2}, \\ &\bar{R} \propto (S_2 - 1)^{1/4}. \end{aligned} \tag{8.3.5}$$

Indeed, closed-form approximations can be written down for such situations:

$$\gamma \simeq \left[\frac{\hat{C}}{L}\mathrm{Ra}_2^{1/3}(T_g - T_2)\right]^2 \frac{C''_{e2}}{4\pi C_{e2}(S_2 - 1)}, \tag{8.3.6}$$

$$M_1 \simeq \frac{\hat{C}A_1}{L}\left(\frac{k\mathrm{Ra}^{1/3}}{H}\right)_1\left(\frac{\xi_1 - \xi_g}{1 + \hat{\mathrm{Cn}}_1}\right) \tag{8.3.7}$$

$$\alpha \simeq \frac{\hat{C}g\rho_L^2 A_s H_1 \mathrm{Ra}_2^{2/3}(T_g - T_2)^2(1 + \hat{\mathrm{Cn}}_1)C''_{e2}}{18\mu_1 L A_1 k_1 \mathrm{Ra}_1^{1/3} C_{e2}(\xi_1 - \xi_g)(S_2 - 1)}. \tag{8.3.8}$$

Then ρ_a and $\bar{R}$ follow, yielding the trends highlighted in (8.3.5), by using (8.2.7), (8.3.3) and (8.3.4).

8.4. Interpolative model

This model, now offered by C-GAS, is named 'interpolative' here because it correctly embraces the two extreme limits of a thick aerosol ('fully coupled') and no aerosol ('uncoupled'), and interpolates for intermediate conditions on the basis of a stagnant boundary-layer model. The equations are [10,11]:

$$f_j = 0, \qquad j = 1, 2, 3, \tag{8.4.1}$$

$$f_1 = S_i - 1 - \frac{\eta C''_{e_i}(1 - \operatorname{sech}\phi)}{4\pi\gamma C_{e_i}}, \tag{8.4.2}$$

$$f_2 = S_i C'_{e_N} - \left(\frac{1 - S_i C_{e_N}}{T_i - T_{N_i}}\right)\ln\left(\frac{1 - S_i C_{e_N}}{1 - C_{e_i}}\right), \tag{8.4.3}$$

$$f_3 = \left(\frac{k}{\rho H\hat{D}}\right)_i \frac{(1 - S_i C_{e_N})}{S_i C'_{e_N}} - \mathrm{Cn}_i, \tag{8.4.4}$$

where

$$\phi = \left[\frac{8\pi\gamma C_{e_i}(S_m - 1)}{\eta C''_{e_i}} \right]^{1/2}, \tag{8.4.5}$$

$$\eta = \left[\frac{q_{ic}}{k\left(1 + \mathrm{Cn}_i^{-1}\right)} \right]^2. \tag{8.4.6}$$

C_{e_i} and C_{e_N} denote $C_e(P, T_i)$ and $C_e(P, T_{N_i})$ respectively, and prime denotes differentiation with respect to temperature. T_{Ni} is the temperature within the boundary layer of surface i at which the supersaturation is equal to S_i. Note that both S_m and ϕ vary from surface to surface.

Equations (8.4.2, 3, 4) thus replace (8.3.1, 2) to make up $3m + 3$ equations for the $3m + 4$ unknowns S_i, Cn_i, T_{N_i}, M_1, γ, α and n_0. As before, one of the unknowns has to be specified.

9. Aerosol optics

The calculations of optical properties require significant computing effort, and the code therefore utilises a look-up table which provides wavelength-averaged optical properties as a function of the droplet size, and during full cover gas calculations C-GAS computations are confined to a summation (as a quadrature) over the aerosol size distribution. This section, the material in which has been extracted from refs. [5,20,21] lists the equations used in all the related computations. C-GAS can generate the look-up table in a separate run, if this is required.

The aerosol particles are assumed to be spherical and to be sufficiently separated in space to permit the neglect of mutual interference in the scattering process. The classical Mie theory can then be used to evaluate the cumulative effect of a given number of particles per unit volume, allowing for size variations.

Consider first a plane, time-harmonic electromagnetic wave of wavelength λ approaching a sphere possessing a radius R and a complex refractive index Φ given by $\Phi_R - i\Phi_I$. Then the Mie theory yields the following expressions for the efficiencies of extinction, scattering and absorption (e.g. [20]:

$$Q_e = \frac{2}{x^2} \sum_{j=1}^{\infty} (2j + 1)\ \mathrm{Re}(a_j + b_j), \tag{9.1}$$

$$Q_s = \frac{2}{x^2} \sum_{j=1}^{\infty} (2j + 1)\left(|a_j|^2 + |b_j|^2 \right), \tag{9.2}$$

$$Q_a = Q_e - Q_s, \tag{9.3}$$

where Re denotes the real part of a complex quantity. The coefficients a_j, b_j are given by

$$a_j = \frac{\psi_j(x)}{\zeta_j(x)} \left[\frac{F_j(y) - \Phi F_j(x)}{F_j(y) - \Phi G_j(x)} \right], \tag{9.4}$$

$$b_j = \frac{\psi_j(x)}{\zeta_j(x)} \left[\frac{\Phi F_j(y) - F_j(x)}{\Phi F_j(y) - G_j(x)} \right], \tag{9.5}$$

where

$$x = 2\pi R/\lambda, \qquad y = \Phi x. \tag{9.6}$$

F_j and G_j are logarithmic derivatives of the Ricatti–Bessel functions ψ_j and ζ_j:

$$F_j(Z) = \frac{\mathrm{d}}{\mathrm{d}Z}\ln \psi_j(Z), \tag{9.7}$$

$$G_j(Z) = \frac{\mathrm{d}}{\mathrm{d}Z}\ln \zeta_j(Z), \tag{9.8}$$

where Z is any complex quantity, and

$$\psi_j(Z) = Zj_j(Z), \tag{9.9}$$

$$\zeta_j(Z) = Zh_j^{(2)}(Z). \tag{9.10}$$

j_j and $h_j^{(2)}$ are Spherical Bessel functions of the first and third kind respectively [30].

Truelove [5] derived the optical constants of the sodium droplets from free electron theory and found good agreement with experimental measurements. The results are

$$\Phi_R^2 - \Phi_I^2 = 1 - \frac{e^2 N_e}{\epsilon_0 m_e(\nu^2 + \hat{\Omega}^2)}, \tag{9.11}$$

$$2\Phi_R\Phi_I = \frac{e^2 N_e \hat{\Omega}}{\epsilon_0 m_e \nu(\nu^2 + \hat{\Omega}^2)}, \tag{9.12}$$

$$\hat{\Omega} = \frac{e^2 N_e}{m_e \sigma_0}, \tag{9.13}$$

where $\nu = 2\pi c/\lambda$, c is the speed of light, N_e is the number of conduction electrons per unit volume, e and m_e are the electronic charge and mass, ϵ_0 is the vacuum permittivity, and σ_0 is the D.C. conductivity. The values of the various parameters in these equations are listed in table 2.

The mean cosine of the scattering angle, denoted here by $\bar{\mu}$, is a measure of the non-isotropy of the scattering phenomenon, and is required for the isotropic scaling:

$$\bar{\mu}Q_s = \frac{4}{x^2}\sum_{j=1}^{\infty}\frac{j(j+2)}{(j+1)}\mathrm{Re}(a_j^* a_{j+1} + b_j^* b_{j+1}) + \frac{4}{x^2}\sum_{j=1}^{\infty}\frac{2j+1}{j(j+1)}\mathrm{Re}(a_j^* b_j), \tag{9.14}$$

Table 2
Parameters used in the evaluation of the optical constants of sodium droplets, obtained from [5,32,33]

Parameter	Meaning	Value
c	Speed of light	3×10^8 m s^{-1}
e	Electronic charge	1.6×10^{-19} C
m_e	Electronic mass	9.11×10^{-31} kg
N_e	Number density of conduction electrons	$(2.647 - 5.894\times10^{-4}\,T_k)\times10^{28}$, m^{-3}
ϵ_0	Permittivity in free space	8.84×10^{-12} F m^{-1}
σ_0	D.C. electrical conductivity	$10^8(-3.34+3.57\times10^{-2}\,T_k - 7.96\times10^{-6}\,T_k^2 + 1.67\times10^{-8}\,T_k^3)^{-1}$, Ω^{-1} m^{-1}

Note: T_k is the temperature in degrees Kelvin.

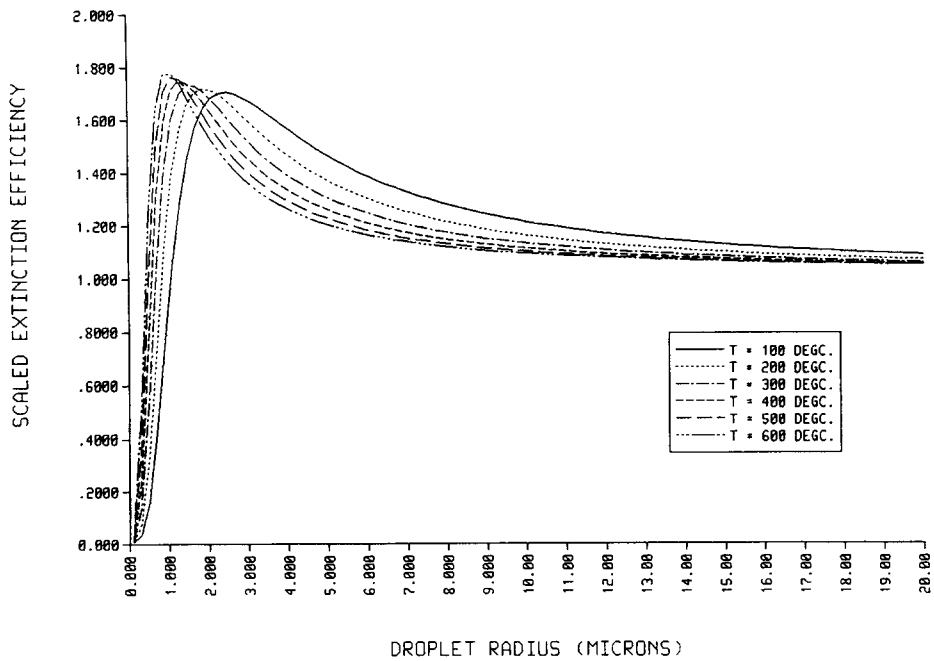

Fig. 8. The wavelength-averaged, isotropically-scaled extinction efficiency $\langle \overline{Q}_e \rangle$ as a function of droplet radius R (microns) and cover gas temperature T_g.

where the asterisk denotes conjugation. The isotropically-scaled quantities are then given by

$$\overline{Q}_e = (1 - \omega\overline{\mu})Q_e, \tag{9.15}$$

$$\overline{\omega} = \left(\frac{1-\overline{\mu}}{1-\omega\overline{\mu}}\right)\omega, \qquad \omega = Q_s/Q_e. \tag{9.16}$$

As mentioned in section 6, the C-GAS model utilises wavelength-averaged optical properties in which the spectrum of the radiation incident on a droplet is assumed to correspond to that of a black body at a temperature T_g. The averaging process for any quantity ψ is defined by

$$\langle \psi \rangle = \frac{\int_0^\infty \psi(\lambda) I_{b\lambda}\, d\lambda}{\int_0^\infty I_{b\lambda}\, d\lambda} \tag{9.17}$$

The denominator is equal to $\sigma T_g^4/\pi$. The numerator is evaluated by the code numerically, when the look-up table is being generated, employing a range of user-supplied temperatures and the range of wavelengths over which the quadrature is to be performed. The code carries out these calculations for a range of user-supplied droplet radii, and then produces a look-up table which lists, for each value of T_g, the values of R, $\langle \overline{Q}_e \rangle$ and $\langle Q_a \rangle$. Figures 8 and 9 depict the variations of $\langle \overline{Q}_e \rangle$ and $\langle \omega \rangle$ with droplet size and temperature. At a radius of 5 microns, the former changes by about 2.5% and the latter by 1% for a temperature increase of 100°C from 400°C; however, variations in the albedo are more important when the latter is close to 1.0, as noted in Section 6.

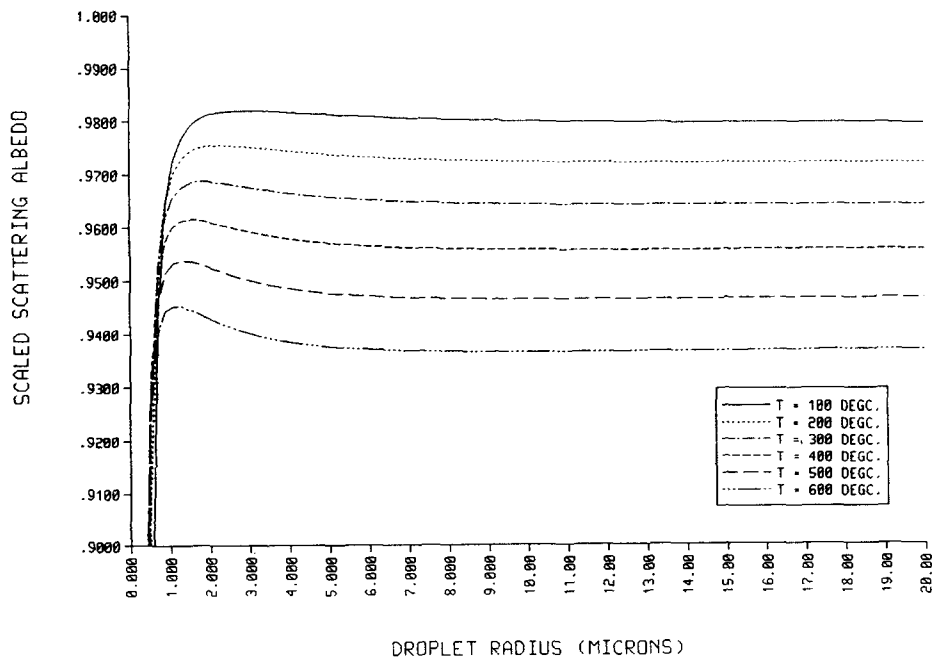

Fig. 9. The wavelength-averaged, isotropically-scaled scattering albedo $\langle \bar{\omega} \rangle$ as a function of droplet radius R (microns) and cover gas temperature T_g.

During actual cover gas runs, C-GAS reads the table, performs linear interpolations in terms of the cover gas temperature T_g and radius R, and evaluates the cloud properties by quadrature as follows:

$$K = \pi \int_0^\infty R^2 n(R) \langle \bar{Q}_e(R) \rangle \, dR, \tag{9.18}$$

$$\omega = K_s/K, \qquad K_s = \pi \int_0^\infty R^2 n(R) \langle \bar{Q}_s(R) \rangle \, dR. \tag{9.19}$$

The code assumes that the size variation is given by the Clement distribution, eq. (8.2.4), which of course evolves as the C-GAS iterations proceed, since n_0 and α are coupled to the whole solution field. The quadrature is performed over a user-specified range of radius.

10. The numerical procedure

As has already been mentioned, the modules which evaluate the behaviour of multiplate arrangements (MPLATE) and the aerosol optical characteristics can be run separately without performing a full cover gas analysis. Additionally, the user has the option of a conventional calculation in which the heat and mass balances are satisfied, or one in which the cover gas temperature is specified and surface fluxes, aerosol characteristics, and net inbalances are determined. The latter facility has been particularly useful in validations against experiments and is exploited by C-GAS-T.

Table 3
NAG routines used by C-GAS

Name	Purpose and comments
C05ADF	(i) Determination of surface temperatures (eq. (5.1.3.)), (ii) Calculation of ν in terms of ω (eq. 6.6).
C05AGF	Global heat and mass balances (eqs. (3.1), (3.2)). This routine is efficient at low roof temperatures but is less robust when the roof is insulated.
C05AZF	Global heat and mass balances (eqs. (3.1), (3.2)). More robust in insulated designs, and requires a search interval.
C05PBF	The interpolative aerosol theory (eqs. (8.4.1), (2) and (3),
E01BEF & E01BFF	Interpolation for the surface conductance h_i at a multiplate arrangement,
S13AAF	Exponential integral, required for the plane-slab expressions of [28].

The bulk of numerical tasks undertaken in C-GAS involve the solution of one or more coupled, non-linear, algebraic equations. In the majority of cases, this is done with the aid of the NAG (Numerical Algorithms Group) library. Either Mark 13 or Mark 14 of that library is compatible with C-GAS. A list of the NAG routines invoked by C-GAS is provided in table 3, together with some explanatory notes.

Information on further development in this area is given in the conclusions at the end of this paper.

Essentially, after performing sundry preliminary calculations, C-GAS iterates for T_g by searching for a zero of a function segment named F2. Within F2, C-GAS first updates the surface temperatures, which of course involves the solution of (5.1.3) using the latest information on view factors etc. Penetration losses are then evaluated with the user-supplied routines. The aerosol inventory (size distribution and moments) is then calculated (eq. (2.2)). This is done by first addressing the surface at which the supersaturation is specified. In the near-equilibrium theory, (8.3.2) provides Cn at that surface, whereupon (8.3.1) yields γ. These two equations subsequently provide S and Cn simultaneously at the remaining surfaces. In the interpolative theory, (8.4.3) is solved for T_N at the 'specified' surface, whereupon (8.4.2, 4) yield Cn at that surface as well as γ. These three equations subsequently give S, T_N and Cn at the remaining surfaces. The inventory then follows from eqs. (8.2.7, 9, 10) and (8.2.4).

The inventory calculations are followed by predictions of the aerosol's optical properties (extinction coefficient and albedo), as well as revisions of the surface-to-surface and surface-to-gas radiative view factors if requested by the code user.

11. Transients: The C-GAS-T code

The fabricated design of the Fast Reactor roof structure consists of concrete blocks separated from a steel shell by cooling passages through which cooling air is forced by pumps during conventional operation. The designer has to assess the structure's thermal-structural response to unusual environments during postulated accidents, accounting for the possibility that LOSSP (Loss of Station Service Power) may occur. The C-GAS-T [31] code is aimed at providing the required thermal information.

The analysis of the reactor steady state is sufficiently complex; the behaviour of the system during transients is even more difficult, since it is necessary to evaluate not only conduction in structures, but also the dynamics of the aerosol inventory. For these reasons, a strategy has been implemented in which C-GAS-T synthesises C-GAS with one-dimensional 'lumped-parameter' models of the steel walls

separating the cover gas from the roof cooling passages, detailed one-dimensional unsteady conduction in the concrete, and with a quasi-steady idealisation of the roof cooling flow; the latter can represent either forced cooling or the natural-convective scenario which is expected to manifest during passive operation.

At present, C-GAS-T divides the roof shell into five regions, and evaluates a mean temperature for each of these. The regions are the bottom roof plate and the penetration walls in the intermediate heat exchanger (IHX), pump (PSP), large rotating plug (LRP) and decay heat exchanger (DHX), and the plates making up any arrangement of insulation suspended beneath the roof plate. The penetration wall is the outer wall bounding the annulus which separates the component and roof. In addition to these five variables, C-GAS-T solves for the cover gas temperature. The set of equations which are integrated by C-GAS-T is therefore

$$\frac{dY_i}{dt} = S_i, \qquad i = 1, 2, \ldots \tag{11.1}$$

$$Y_1 = T_g, \qquad Y_2 = T_r, \qquad Y_3 = T_{IHX}, \qquad Y_4 = T_{PSP}, \qquad Y_5 = T_{LRP}, \qquad Y_6 = T_{DHX}. \tag{11.2}$$

$$S_i = \bar{q}_i/\bar{C}_i, \qquad \bar{q}_1 = Q, \qquad \bar{C}_1 = \rho C_p V. \tag{11.3}$$

In the equation $i = 1$, Q is the net energy imbalance of the cover gas (watts); C-GAS-T relies on a system code to supply the various sodium temperatures as a function of time. The variations in thermosyphonic losses are accounted for in Q, as explained below. The quantities ρ, C_p and V are the mean density and specific heat of the cover gas, and V is its volume.

In eq. (11.1) for $i > 1$, $\bar{q}_i$ represents the net heat gained by the pertinent wall per unit area, viz. the flux gained from the cover gas side minus the flux lost to the cooling system. It is written as

$$\bar{q}_i = q_{iI} - q_{i0}, \tag{11.5}$$

$$\bar{C}_i = \rho_i C_i L_i. \tag{11.6}$$

Here ρ_i, C_i and L_i are the steel density, specific heat and thickness respectively. The transients are assumed to be sufficiently slow to permit the quasi-steady formulation embodied in (11.1).

A schematic diagram of the C-GAS-T structure is provided in fig. 10.

Initial conditions are delivered to C-GAS-T by a steady-state C-GAS run, in addition to a number of further parameters specified by the user. The C-GAS run provides Y_{1o} and Y_{2o} directly (the subscript zero denotes condition at $t = 0$).

Consider unidirectional channel flow in which a fluid accepts heat from an isothermal wall. If it is assumed that the channel is sufficiently long to preclude entry effects, and that the heat transfer coefficient h is constant, then energy conservation yields the usual

$$\frac{T_0 - T_b}{T_w - T_b} = 1 - \exp(-\chi), \qquad \chi = \frac{Ah}{WC_p}. \tag{11.7}$$

Here T_b, T_0, T_w are flow inlet and outlet temperatures and the wall temperature respectively. A is the wetted area (viz. the perimeter multiplied by the conduit's length), and W is the mass flow rate. This relation is applied to each of the penetrations at the initiation of the transient by noting that during

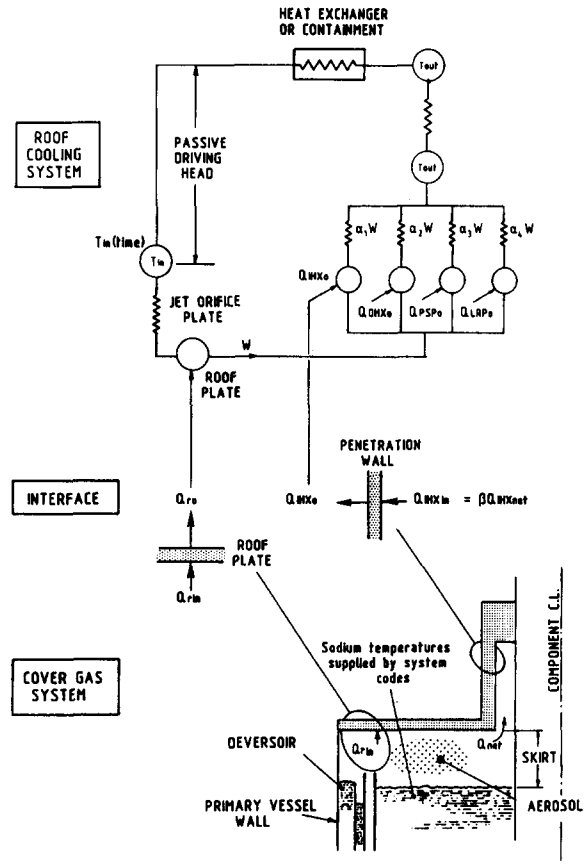

Fig. 10. Sketch of the C-GAS-T modelling strategy.

normal operation $\bar{q}_i = 0$, and the mean outlet temperature in the cooling channel adjacent to a particular penetration is given by

$$T_0 = T_b + Q_i/W_i C_p. \tag{11.8}$$

Here T_b is the inlet temperature at the base of the penetration, given by

$$T_b = T_c + Q_r/WC_p, \tag{11.9}$$

where T_c is the roof cooling inlet temperature, and Q_r and W are the normal-operation roof-plate heat loading and total cooling flow rate (kg s^{-1}) respectively. Q_i is total heat delivered to penetration of type i, and W_i is the cooling flow rate of that part of the cooling system which is adjacent to that wall. It is important to observe that the heat delivered to the penetration wall is not necessarily equal to the net heat exchanged with the cover gas, since some components are hot and capable of delivering additional heat, principally by radiation. In fact, C-GAS-T assumes

$$Q_i = \beta_i Q_{i_{net}}; \tag{11.10}$$

where $Q_{i_{net}}$ is the net heat exchanged with the cover gas, and β_i (> 1) is postulated to remain constant throughout the transient.

The initial wall temperature is now defined by insisting that when this 'mean' value is used in eq. (11.7), it yields an outlet temperature which is consistent with (11.8):

$$T_{w_0} = \tilde{T}_{b_0} + \frac{Q_{i_0}}{\tilde{W}_{i_0} C_p [1 - \exp(-\chi_{i_0})]}. \tag{11.11}$$

The tilda's are used here on T_b, χ, and W_i in order to emphasise that these quantities change rapidly at $t = 0$, and indeed, in the present model they change discontinuously since new values are calculated at $t = 0$ when the cooling fans are assumed to lose their power. Thus $\tilde{T}_{b_0}$, χ_0 and $\tilde{W}_{i_0}$ are the values which apply immediately *before* the initiation of the event, and T_{b_0}, χ_0 and W_{i_0} are the value *calculated* immediately *after* the initiation.

Values of $\tilde{T}_{b_0}$, χ_0, $\tilde{W}_{i_0}$ and Q_{i_0} are evaluated from the initial C-GAS run as well as the roof cooling and thermosyphon calculations. Moreover, the isothermal cooling calculations have provided the flow splits along the penetrations:

$$W_i = \alpha_i W, \qquad i = 3, 4, 5, 6. \tag{11.12}$$

For the present, it is assumed that the α_i's remain constant throughout a transient. The full roof cooling network model has indicated that this assumption is a reasonable one, whether or not Reynolds number effects are taken into account.

The C-GAS code is required by C-GAS-T during the transient for several reasons:

(i) The cover gas energy source Q is required for S_1. Whilst it is true that the cover gas relaxation time without aerosol effects is relatively short (of the order of 10 seconds), it is not obvious at this stage how aerosol dynamics influences these characteristics, and a decision was therefore made early in the C-GAS-T development to include T_g as a dependent variable, rather than to evaluate T_g via $Q = 0$ (as is done by C-GAS for steady state).

(ii) q_{i_1} is required for all the modelled surfaces. In order to evaluate Q and the heat fluxes at bounding surfaces, C-GAS needs to know the current values of the cover gas temperature, the temperature of bounding surfaces, and the penetration losses. The temperature of the roof plate is known because it is a dependent variable which is integrated by C-GAS-T. Of the remaining surfaces, the sodium hot and cold pools are considered the most important with values read in from the input data file. The sodium data has to be supplied from a separate system code.

In order to estimate the transient penetration losses, it has been assumed that the net loss of a penetration scales on Ra ^{b}, where Ra is a Rayleigh number based on the current temperature difference between the cover gas and the 'mean wall'. Thus,

$$Q_{i_{net}} = Q_{i_{net_0}} \left(\frac{Y_2 - Y_i}{Y_{2_0} - Y_{i_0}} \right)^b, \quad i = 3, 4, 5, 6; \tag{11.13}$$

b is an index, expected to lie between 1 and 4/3 (the former value is used presently). The flux in eq. (11.5) is defined by

$$q_{i_1} = Q_i / (\text{area of penetration wall}). \tag{11.14}$$

The scaling thus provides the thermosyphonic loses (eq. (11.13)) for the benefit of C-GAS and the heat input to the penetrations (eq. (11.14)) for the benefit of C-GAS-T itself.

An important constraint which applies to current C-GAS-T calculations is the assumption that the cover gas is either transparent or optically thick throughout the transient. This will be relaxed when ongoing cover gas experiments and C-GAS validation are completed.

During passive operation, the roof cooling flow rate is determined from a balance of the sum of singular and viscous losses on the one hand, and the hydrostatic driving head on the other:

$$\frac{\hat{R}}{\rho_r} W^2 - gH(\rho_c - \rho_{out}) = 0. \tag{11.15}$$

W is the air mass flow rate through the whole roof and H is the effective driving head. For example, if the chosen design possesses a chimney to promote cooling by natural circulation, it is assumed that the chimney is insulated and the driving head is the difference in height between the top of the roof slab and the chimney's outlet. ρ_c is the density of the cooling air as it enters the roof slab, ρ_{out} is its density as it exits the slab, and ρ_r is a reference (mean) density. For convenience, the resistance $\hat{R}$ is decomposed into a component R_1 representing the resistance of the roof slab and R_2 standing for the remainder of the circuit, outside the slab:

$$\hat{R} = \hat{R}_1 + \hat{R}_2. \tag{11.16}$$

$\hat{R}_1$ and $\hat{R}_2$ can vary with flow, and are indeed supplied by the user within the input data file. C-GAS-T determines W iteratively from equation (11.15) and simultaneously evaluate the Q_{i_0}'s required by S_i. Following a guess of W, given the current state of the slab, heat transfer coefficients are evaluated at the roof plate and all the penetration cooling passages using mixed-convection correlations and representing low Reynolds number effects. Thus,

$$q_{2_0} = h_2(Y_2 - T_c) + \sigma F_2\left(T_2^4 - \hat{T}_c^4\right). \tag{11.17}$$

T_c is the cooling inlet temperature, supplied by the user as a function of time. The second term in (11.17) represents thermal radiation between the roof plate and the concrete; the temperature of the latter at its interface with the cooling air is $\hat{T}_c$, and F_2 is an appropriate view factor. The temperature profile within the concrete is obtained by a finite-difference TDMA solution of the one-dimensional diffusion equation. A similar treatment is used at all the penetrations. It is possible to iterate manually between C-GAS-T and the containment code, but ultimately it would be preferable to couple the two codes fully.

The quantity Q_r in equation (11.9) is just the roof-plate area multiplied by equation (11.17). Hence T_b is known, and equation (11.7) then provides the flow outlet temperature at each penetration. The mixed outlet temperature is then determined as the mixed mean value of the constituent flows, and this fixes ρ_{out}. W is changed until (11.15) is satisfied.

Note that application of eq. (11.7) quantifies the amount of heat surrendered by the penetration walls to the cooling flow (see eq. (11.8)) and, by division by the appropriate areas, the values of the flux q_{i_0} and the source terms S_i; the integration of eqs. (11.1) may then proceed.

12. Conclusions

This paper outlines the UK's calculational strategy for the cover gas analysis and lists the equations which are solved by C-GAS. Some of the supporting modules are included in C-GAS itself, and details thereon have been provided here, but some modules are run separately to provide look-up tables or input routines, and in these cases this report has been confined to brief introductory descriptions and identification of pertinent references.

The theory underlying the C-GAS model benefits from the aim of representing the real physical phenomena, and is therefore sufficiently flexible to address fundamentally different designs. However, the aerosol modelling awaits a closure to the equation set, and it is therefore most important that studies

of nucleation phenomena should continue. Meanwhile, on-going experiments, in which simultaneous aerosol and heat transfer measurements are made, play a vital role in clarifying this difficulty before a successful nucleation theory is developed. Applications of the theory need to account for the complex phenomena affecting surface emissivities (e.g. [38]).

As far as further C-GAS developments are concerned, it is necessary to account for aerosol removal and redistribution mechanisms other than gravitational settling, and work on C-GAS validation must continue. These activities will be reported in due course.

While this paper was in print, the numerical algorithms were modified at Harwell to permit self-standing execution without any of the NAG routines. This version of the code, which is more robust (especially in optically thin situations), has been satisfactorily tested on a personal computer, a work-station, and a mainframe. Additionally, improvements to the aerosol modelling have been initiated. Work has begun on a paper illustrating the application of C-GAS [32].

Appendix I. Physical properties

The following equilibrium properties have been obtained from [33–37]. T_k and T_c are the temperature in degrees Kelvin and Celsius respectively, and P is the absolute pressure in bars. The subscripts v and g appertain to the vapour (sodium) and inert gas (argon) respectively.

(1) Sodium liquid density

$$\rho_L = 949 - 0.223\ T_c - 1.75 \times 10^{-5}\ T_c^2. \tag{I.1}$$

(2) Sodium vapour pressure and density

$$P_v = 1.013 \times 10^5 \exp\left[\frac{-12818}{T_k} - 0.5 \ln(T_k) + 14.6306\right] \quad [\mathrm{Pa}], \tag{I.2}$$

$$\rho_v = 1000 \exp(-1/z) \quad [\mathrm{kg\ m^{-3}}], \tag{I.3}$$

$$z = 1.91711 \times 10^{-8}\ T_k^2 + 8.4563 \times 10^{-5}\ T_k - 7.3053 \times 10^{-4}. \tag{I.4}$$

(3) Sodium latent heat of vaporisation

$$H = 4.1993 \times 10^6 - 985.58\ T_k \quad [\mathrm{J\ kg^{-1}}]. \tag{I.5}$$

(4) Argon pressure and density

$$P_g = 10^5\ P - P_v \quad [\mathrm{Pa}], \tag{I.6}$$

$$\rho_g = \frac{P_g}{208.18\ T_k} [\mathrm{kg\ m^{-3}}]. \tag{I.7}$$

(5) Expansion coefficient

$$\beta = T_k^{-1} \quad [\mathrm{K^{-1}}]. \tag{I.8}$$

(6) Gas–vapour mixture density

$$\rho = \rho_g + \rho_v \quad [\mathrm{kg\ m^{-3}}]. \tag{I.9}$$

(7) Specific heats

$$C_{p_v} = 900, \quad C_{p_g} = 520.6 \quad [\mathrm{J\ kg^{-1}\ K^{-1}}], \tag{I.10}$$

$$C_p = (1 - C_e)C_{p_g} + C_e C_{p_v} \quad [\mathrm{J\ kg^{-1}\ K^{-1}}], \tag{I.11}$$

$$C_e = \rho_v/\rho. \tag{I.12}$$

(8) Gas conductivity (neglect vapour)

$$k = 1.6343 \times 10^{-2} + 5.3243 \times 10^{-5}\ T_c - 6.2857 \times 10^{-8}\ T_c^2 + 1.4425 \times 10^{-10}\ T_c^3 - 2.2135 \times 10^{-13}\ T_c^4 + 1.7096 \times 10^{-16}\ T_c^5 - 5.0498 \times 10^{-20}\ T_c^6 \quad [\mathrm{W\ m^{-1}\ K^{-1}}]. \tag{I.13}$$

(9) Gas viscosity (neglect vapour)

$$\mu = 2.1244 \times 10^{-5} + 6.4081 \times 10^{-8}\ T_c - 5.1874 \times 10^{-11}\ T_c^2 + 6.5606 \times 10^{-14}\ T_c^3 - 5.9325 \times 10^{-17}\ T_c^4 + 2.9606 \times 10^{-20}\ T_c^5 - 5.7636 \times 10^{-24}\ T_c^6 \quad [\mathrm{N\ s\ m^{-2}}]. \tag{I.14}$$

(10) Gas mixture kinematic viscosity

$$\hat{\nu} = \mu/\rho \quad [\mathrm{m^2\ s^{-1}}]. \tag{I.15}$$

(11) Gas mixture thermal diffusivity

$$\hat{\lambda} = k/\rho C_p \quad [\mathrm{m^2\ s^{-1}}]. \tag{I.16}$$

(12) Vapour-argon binary mass diffusivity (Moulaert, cf. [36])

$$\hat{D} = 5.16 \times 10^{-9}\ T_k^{3/2}/P \quad [\mathrm{m^2\ s^{-1}}]. \tag{I.17}$$

Acknowledgements

YLS wishes to thank J. Davidson for many inspiring discussions, the NNC library staff for their assistance, J Young for the typing, and NNC for permission to publish this paper. The transient concrete conduction algorithm was synthesised with the C-GAS-T code by Dr W U A Leong. Helpful comments on this paper were made by G Costigan (AEA, Harwell).

Nomenclature

a_j Mie coefficient, eq. (8.4),
A wetted cross-sectional area in a roof cooling passage, eq. (11.7) [m^2],
A_i area of ith surface of the boundary of the cover gas domain [m^2],
A_s total horizontal, or horizontally projected area available for gravitational settling of the aerosol [m^2],
b_j Mie coefficient, eq. (9.5),
C non-equilibrium sodium vapour mass fraction, ρ_v/ρ,

$\hat{C}$ constant, eq. (4.3),
$C_e(P, T)$ Equilibrium value of C at a pressure P and temperature T,
C_{e_i} $C_e(P, T_i)$,
C_{eN} $C_e(P, T_{N_i})$,
C_i specific heat of ith region in C-GAS-T [J kg^{-1} K^{-1}],
$\overline{C}_i$ thermal inertia, eq. (11.6), [J m^{-2} K^{-1}],
Cn surface condensation number, eq. (8.1.2),
$\hat{\text{Cn}}$ equilibrium value of Cn,
C_p gas equilibrium specific heat at constant pressure [J kg^{-1} K^{-1}],
D droplet diameter [m],
$\hat{D}$ vapour-argon binary mass diffusivity [m^2 s^{-1}],
e electronic charge [C],
E_i evaporative mass flux at surface i (a negative value denotes condensation) [kg m^{-2} s^{-1}],
f_j interpolative aerosol equations (8.4.1),
F plate-to-plate view factor, eq. (5.2.5),
F_i view factor for radiative exchange between surface i and a source at temperature $\hat{T}_g$ on the 'cover gas side',
F_{ic} view factor for radiative exchange between surface i and a source at temperature T_{ic} on the 'sink side', eq. (5.1.3),
F_{ig} view factor for radiative exchange between surface i and the aerosol (see eq. 6.2),
F_{ij} view factor for radiative exchange between surface i and surface j, accounting for the influence of the aerosol. F_{ij} is defined in such a way that the total heat arriving at surface j from surface i is $\sigma A_j F_{ij} (T_i^4 - T_j^4)$,
F_j logarithmic derivative of ψ_j, eq. (9.7),
g gravitational acceleration [m s^{-2}],
G_j logarithmic derivative of ζ_j, eq. (9.8),
h heat transfer coefficient, or conductance [W m^{-2} K^{-1}],
h_{ig} convective heat transfer coefficient at surface i, eqs. (4.1) and (4.3) [W m^{-2} K^{-1}],
h_{is} conductance representing an additional linear source at temperature T_{is} supplying heat to surface i from the cover gas side [W m^{-2} K^{-1}],
$h_j^{(2)}$ spherical Bessel function of the third kind [28],
H Sodium latent heat of evaporation, or the height difference eq. (11.5) [J kg^{-1}],
i $(-1)^{1/2}$,
I total radiation intensity [W m^{-2} sr^{-1}],
I_b total black-body intensity, $\sigma T^4/\pi$ [W m^{-2} sr^{-1}],
$I_{b\lambda}$ Planck's function for the spectral black-body intensity, $C_1/\{\lambda^5[\exp(C_2/\lambda T) - 1]\}$, $C_1 = 11.908 \times 10^{-17}$ W m^2 sr^{-1}, $C_2 = 1.439 \times 10^{-2}$ m K [W m^{-3} sr^{-1}],
I_λ spectral radiative intensity [W m^{-3} sr^{-1}],
j_j spherical Bessel function of the first kind [28],
k gas thermal conductivity [W m^{-1} K^{-1}],
k_s thermal conductivity of the 'bridging' material, in a multiplate arrangement, eq. (5.2.2) [W m^{-1} K^{-1}],
K size- and wavelength-averaged, isotropically-scaled extinction coefficient $K_a + K_s$, eq. (9.18) [m^{-1}],
K_a absorption coefficient [m^{-1}],
K_s scattering coefficient [m^{-1}],
L reference length [m],
m number of surfaces facing the cover gas at the boundary,

$\hat{m}$ constant, eq. (4.3),

m' number of surfaces at which phase change is taking place. In C-GAS, $m' = m$ and the user specifies those surfaces at which phase change is represented,

m_e electronic mass, see table 2 [kg],

M_j jth sodium mass sink, other than condensation at a surface [kg s^{-1}],

M_1 aerosol mass sink due to gravitational settling, eq. (8.2.9) [kg s^{-1}],

n number of 'extraneous' energy sources, eq. (3.1),

$n(R)$ droplet size distribution, such that the number of droplets per unit volume possessing radii between R and $R + dR$ is $n(R)\,dR$ [m^{-4}],

n' number of sodium mass sinks, eq. (3.2),

n_0 parameter in aerosol size distribution, eq. (8.2.4) [m^{-3}],

N total aerosol number density, eq. (8.2.1) [m^{-3}],

Nu Nusselt number, hL/k or $h_{ig}L/k$,

p scattering phase function, eq. (6.1),

P total gas pressure [Pa],

P_g argon partial pressure [Pa],

Pr Prandtl number, $\hat{\nu}/\hat{\lambda}$,

P_v sodium vapour partial pressure [Pa],

q_i total heat flux passing through surface i, positive when energy is flowing from the cover gas side towards the sink side [W m^{-2}],

q_{ic} convective (sensible plus latent) heat flux at surface i eqs. (3.1, 4.1) [W m^{-2}],

q_{ig} total heat flux delivered to those parts of surface i which are facing the cover gas eq. (5.1.2). This differs from q_i if a protruding structure also delivers heat to the surface (cf. q_{is}) [W m^{-2}],

q_{il} heat flux delivered from the cover gas to the ith region in C-GAS-T [W m^{-2}],

q_{il} latent heat flux at surface i [W m^{-2}],

q_{i0} heat flux removed by the roof cooling system from the ith region in C-GAS-T [W m^{-2}],

q_{is} additional linear heat flux delivered to surface i from the cover gas, eq. (5.1.5) [W m^{-2}],

$Q_{a,e,s}$ absorption, extinction and scattering efficiencies for a single sphere, eqs. (8.1, 2, 3),

$\underline{Q}$ Net energy imbalance in the cover gas under transient conditions [W],

$\bar{Q}$ isotropically-scaled efficiency, eqs. (9.15, 16),

Q_j jth gas blanket heat source. Roof thermosyphons would be represented by negative values [W],

R droplet radius [m],

$\hat{R}$ cooling system's flow resistance [m^{-4}],

Ra Rayleigh number, $g\beta\,\Delta T L^3/\hat{\nu}\hat{\lambda} = \mathrm{Gr\,Pr}$,

S vapour supersaturation, C/C_e,

$\hat{S}$ vapour supersaturation, P_v/P_{ve},

$\tilde{S}$ source term in the aerosol eq. (8.2.4) [m^{-4} s^{-1}],

T_c roof cooling inlet temperature [K],

T_g bulk cover gas temperature [K],

T_i temperature at the interface between the cover gas and the ith surface [K],

T_{ic} temperature of linear sink at surface i, eq. (5.1.1) [K],

$\hat{T}_{ic}$ temperature of radiative sink at surface i, eq. (5.1.3) [K],

$\hat{T}_{ig}$ temperature of additional radiative source delivering heat to surface i from the cover gas side [K],

T_{is} temperature of the linear source supplying heat to surface i from the cover gas side (see q_{is} and eq. (5.1.5)) [K],

T_{Ni} the temperature in the ith boundary layer at which the supersaturation is a maximum [K],

T_w mean wall temperature, $w = r$, IHX, PSP, LRP, DHX in C-GAS-T [K],
V cover gas volume [m^3],
W roof cooling mass flow [kg s^{-1}],
$\boldsymbol{x}$ position vector [m],
x $2\pi R/\lambda$,
y Φx,
Y_i ith variable in C-GAS-T,
z eq. (I.3).

Greek

α aerosol size distribution parameter, eq. (7.2.4) [m^{-4}],
$\hat{\alpha}$ fraction, in terms of the whole area of surface i, which is occupied by a structure protruding into the cover gas region,
α_i roof cooling flow distributions past each type of penetration, assumed to be constant,
β isobaric expansion coefficient of the gas [K^{-1}],
β_i eq. (11.10),
γ $N\bar{R}$,
ΔT temperature difference [K],
ϵ_i total hemispherical emissivity of surface i,
ϵ_g effective aerosol emissivity in the optically-thick limit, eq. (6.5),
ϵ_0 permittivity in vacuo [F m^{-1}],
ζ_j Ricatti-Bessel function eq. (9.10),
η eq. (8.4.5) [K^2 m^{-2}],
θ_1 $1 - \text{sech}\phi\ (1 + \frac{1}{2}\phi \tanh \phi)$,
θ_2 $1 - S_i C_{e_N}$,
θ_3 $\ln[\theta_2/(1 - C_{ei})$,
λ wavelength of light [m],
$\hat{\lambda}$ thermal diffusivity, $k/\rho C_p$ [m^2 s^{-1}],
μ dynamic viscosity [kg m^{-1} s^{-1}],
$\bar{\mu}$ mean cosine of scattering angle, eq. (9.14),
ν parameter in optically-thick radiation model, eqs. (6.5, 6.6), or $2\pi C/\lambda$ eqs. (9.11, 12),
$\hat{\nu}$ momentum diffusivity [m^2 s^{-1}],
ξ $T + C_e H/C_p$ [K],
ρ density, $\rho_v + \rho_g$ [kg m^{-3}],
ρ_g argon density [kg m^{-3}],
ρ_v sodium vapour density [kg m^{-3}],
σ Stefan-Boltzmann constant, 5.67×10^{-8} [W m^{-2} K^{-4}],
σ_0 zero-frequency electrical conductivity [Ω^{-1} m^{-1}],
ϕ eq. (8.4.4),
Φ droplet refractive index, $\Phi_R - i\ \Phi_I$,
χ eq. (11.7),
ψ_j Ricatti–Bessel function, eq. (9.9),
ω size- and wavelength-average, isotropically scaled scattering albedo, eq. (9.19),
$\hat{\omega}$ eq. (9.16),
$\boldsymbol{\Omega}$ direction vector [rad s^{-1}],
$\hat{\Omega}$ electron damping frequency, eq. (9.13),

Subscripts

a aerosol,
e equilibrium,
g argon,
i at surface number *i*,
L liquid sodium,
m maximum possible value,
v sodium vapour.

References

[1] A.J. Judd, Fast Breeder Reactors (Pergamon, London, 1981).
[2] B. Klemme et al., Vol. 1, Paper 115, Avignon, 17-21 October 1988 (SFEN, Paris 1988).
[3] J. Davidson, Private communication (1988).
[4] C.F. Clement and P. Hawtin, Proc. Int. Conf. on Liquid Metal Technology in Energy Production, Ed. M.H. Cooper, Seven Springs, Pennsylvania, 1976, p. 603.
[5] J.S. Truelove, Int. J. Heat and Mass Transfer 27, No. 11 (1984) 2085–2093.
[6] C.F. Clement, Proc. R. Soc. Lond. A398 (1985) 307–339.
[7] C.F. Clement, Proc. Heat and Mass Transfer in the Reactor Cover Gas, Harwell, 8-10 October 1985, paper no. 2/2, IWGFR-57, IAEA (1985).
[8] J.C. Barrett and C.F. Clement, Proc. Heat and Mass Transfer in the Reactor Cover Gas, Harwell, 8-10 October 1985, paper no. 2/1, IWGFR-57, IAEA (1985).
[9] J.C. Barrett and C.F. Clement, AERE TP. 1305 (1988).
[10] I.J. Ford and C.F. Clement, AERE TP. 1354 (1990).
[11] I.J. Ford, Unpublished AEA report (June 1990).
[12] Y.L. Sinai, NNC unpublished reports (June 1988 and September 1991).
[13] G. Lemercier, Proc. Second. Int. Meeting on Liquid Metal Technology in Energy Production, Richland, 20–24 April 1980, ANS.
[14] Y. Himeno and J. Takahashi, J. Nucl. Sci. Technol. 17, No. 6 (1980) 404–412.
[15] P. Pradel, S. Frachet and D. Petit, Proc. Third Int. Conf. Liquid Metal Engineering and Technology, Vol. 1, Oxford, 9-13 April 1984, BNES (1984), 459-462.
[16] O. Furukawa et al., Proc. Third Int. Conf. Liquid Metal Engineering and Technology, Vol. 1, Oxford, 9-13 April 1984, BNES (1984), 451-458.
[17] N. Hattori, A. Furutani and O. Furukawa, Proc. Heat and Mass Transfer in the Reactor Cover Gas, Harwell, 8-10 October 1985, paper no 5/4, IWGFR-57, IAEA (1985).
[18] M. Julien-Dolias, Fourth Int. Conf. Liquid Metal Engineering and Technology, Vol. 1, paper no. 113, Avignon, 17-21 October 1988 (SFEN, Paris 1988).
[19] W. Schütz and J. Minges, Fourth Int. Conf. Liquid Metal Engineering and Technology, Vol. 1, paper no 114, Avignon, 17-21 October 1988 (SFEN, Paris 1988).
[20] H.C. Hottel and A.F. Sarofim, Radiative Transfer (McGraw-Hill, New York, 1967).
[21] R. Siegel and J.R. Howell, Thermal Radiation Heat Transfer, Second Edition (Hemisphere/McGraw-Hill, New York, 1981).
[22] I. Kinoshita et al., Fourth Int. Conf. Liquid Metal Engineering and Technology, Vol. 1, paper no. 112, Avignon, 17-21 October 1988 (SFEN, Paris 1988); also I. Kinoshita, CRIEPI Report ET87004 (July 1987).
[23] Y.L. Sinai, NNC unpublished report (February 1991).
[24] K. Freudenstein, Proc. Heat and Mass Transfer in the Reactor Cover Gas, Harwell, 8-10 October 1985, paper no. 6/3, IWGFR-57, IAEA (1985).
[25] K. Freudenstein and H.J. Friedrich, ENC86 Transactions, Vol. 2, Geneva, 1-6 June, 1986, Nuclear Energy of Today and Tomorrow, 783-788.
[26] A.W.D. Hills and J. Szekely, Chem. Engrg. Sci. 19, No. 1 (1964) 79–81.
[27] H. Lee and R.O. Buckius, J. Heat Transfer 104, No. 1 (1982) 68–75.
[28] M.M.R. Williams, IMA J. Appl. Math. 31 (1983) 37–50; also IMA J. Appl. Math. 33 (1984) 101–103.
[29] R.B. Bird, W.E. Stewart and E.N. Lightfoot, Transport Phenomena (Wiley, New York, 1960).
[30] M. Abramowitz and I.A. Stegun, Handbook of Mathematical Functions (Dover, New York, 1965).
[31] Y.L. Sinai, NNC unpublished report (July 1990).

[32] M. Sittig, Sodium: Its Manufacture, Properties and Uses (Chapman & Hall, London, 1956).
[33] J.W. Mausteller, F. Tepper and S.J. Rodgers, Alkali Metal Handling and Systems Operating Techniques (Gordon & Breach, London, 1967).
[34] A.E. Jenkins, UKAEA unpublished report (1977).
[35] E.L. Dunning, AEC Research & Development Report, ANL-6246 (October 1960).
[36] T. Kumada, R. Ishiguro and Y. Kimachi, Nucl. Sci. Engrg. 70 (1979) 73–81.
[37] Y.L. Sinai, I.J. Ford, J.C. Barrett, C.F. Clement and B.N.O. Hoyal, in preparation.
[38] J.D. Jackson, D.K.W. Tong, P.G. Barnett and P. Gentry, Nucl. Energy 26 (1987) 387–392.